

The Nanocaterpillar’s Walk: Diffusion With Ligand-Receptor Contacts

Sophie Marbach,^{1,2} Jeana Aojie Zheng,³ and Miranda Holmes-Cerfon¹

¹*Courant Institute of Mathematical Sciences, New York University, NY, 10012, U.S.A.*

²*CNRS, Sorbonne Université, Physicochimie des Electrolytes et Nanosystèmes Interfaciaux, F-75005 Paris, France* *

³*Department of Physics, New York University, NY, 10012, U.S.A.*

Particles with ligand-receptor contacts span the nano to micro scales in biology and artificial systems. Such “nanoscale caterpillars” bind and unbind fluctuating “legs” to surfaces, whose fluctuations cause the nanocaterpillar to diffuse over long timescales. Quantifying this diffusion is a challenge, since binding events often occur on very short time and length scales. Here we present a robust analytic framework, validated by simulations, to coarse-grain these fast dynamics and obtain the long time diffusion coefficient of a nanocaterpillar in one dimension. We verify our theory experimentally, by measuring diffusion coefficients of DNA-coated colloids on DNA-coated surfaces. We furthermore compare our model to a range of other models and assumptions found in the literature, and find ours is the most general, encapsulating others as special limits. Finally, we use our model to ask: when does a nanocaterpillar prefer to move by *sliding*, where one leg is always linked to the surface, or by *hopping*, which requires all legs to unbind simultaneously? We classify a range of nanocaterpillar systems (viruses, molecular motors, white blood cells, protein cargos in the nuclear pore complex, bacteria such as *Escherichia coli*, and DNA-coated colloids) according to whether they prefer to hop or slide, and present guidelines for materials design.

Particles with ligand-receptor contacts – or *nanocaterpillars* – harvest binding and unbinding dynamics of their fluctuating *legs* at the nanoscale to move, target, stick, or assemble into large structures [1–4]. Nanocaterpillars are found across multiple scales, spanning a great variety of systems in biology and biomimetic assays – see Fig. 1-A. To name but a few, microscale white blood cells with protein linkers stick and roll on blood vessel walls until they reach a healing target [5–7]. Microscale droplets with protein linkers are used to study cellular-like adhesion [8–10]. Micronscale down to nanoscale colloids coated with complementary deoxyribonucleic acid (DNA) strands may self-assemble into macroscopic crystals [4, 11, 12] with novel optical or selectivity properties [13–16]. Nanoscale viruses transiently adhere with spike proteins to the respiratory mucus to find vulnerable host cells [1, 17–19]. At even smaller scales, protein cargos bind to receptors in the nuclear pore complex for selective transport to a cell’s nucleus [20, 21].

For all these systems to function, a nanocaterpillar must *move* relative to the surface to which its legs are attracted. An important question therefore is to characterize *how* it moves, over scales much larger than individual legs. Since legs constantly bind and unbind to the surface, imparting force each time they do so, the particle’s macroscopic mobility depends on the microscopic details of its legs. For example, leg flexibility and bond lifetimes control the average mobility of the particle [19, 23, 24], and differences in both parameters can be harvested to detect infected cells [25–27] or prevent viral infections [28]. Leg density affects how DNA-coated colloids nucleate and grow into crystals [29, 30] and governs the long-range alignment of crystals [31–33]. Overall, microscopic details underlie a variety of large-scale modes of

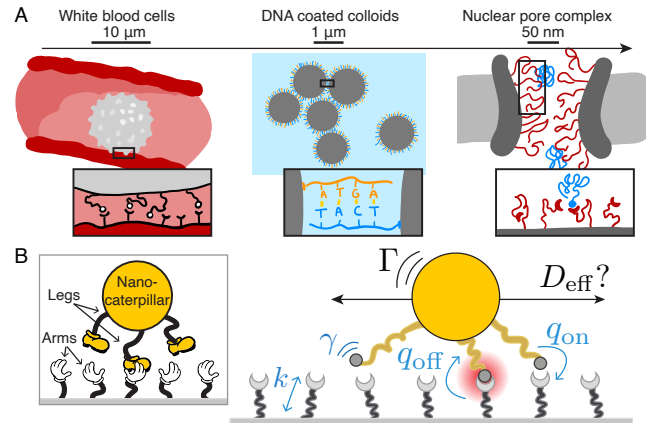


FIG. 1. Overview of nanocaterpillars. (A) Multivalent ligand-receptor systems span the micro to nanoscales. White blood cells stick to vessel walls through selectin mediated bonds (inspired from Ref. [7]); DNA-coated colloids self-assemble through hybridization of complementary DNA strands; Protein cargos translocate through the polymer mesh of the nuclear pore complex (inspired from Ref. [22]). (B) Ligand-receptor systems are modelled here with an arbitrary number of legs (ligands) and/or arms (receptors). The stochastic model includes binding and unbinding rates q_{on} and q_{off} , spring constant k , and leg friction γ (all fast, in blue); and the bare friction coefficient Γ of the nanocaterpillar (slow, in black). We seek the long-time effective longitudinal diffusion coefficient D_{eff} .

motion, such as hopping [3, 17, 34, 35], cohesive motion including rolling and crawling [17, 36], and also transient or firm arrest [3, 5, 37], resulting in large differences in macroscopic mobility.

Investigating how microscopic binding details lead to macroscopic mobility is challenging, as it requires probing time and length scales that can often be quite different [19, 38] – legs can be much smaller than the

* sophie@marbach.fr

nanocaterpillar they are attached to, while leg dynamics can be orders of magnitude faster than the timescales of macroscopic motion. Furthermore, many systems have a valency of thousands of leg contacts [31, 38, 39], too many degrees of freedom to resolve experimentally or computationally [22, 40]. To make progress, numerical and analytical models often rely on simplified assumptions, *e.g.* excluding stochastic relaxation of the legs [41, 42], limiting the analysis to a small number of legs [41, 43, 44], or assuming the perturbation to mobility is small compared to the background mobility [22]. Such models have given insight into a variety of phenomena, such as how specific parameters could favor rolling over sliding motions [7, 41, 43, 45, 46] or how specific mechanisms could increase overall particle mobility (through leg cooperativity [47, 48] or using binding rates with multiple adhesive sites [22, 49, 50]). Nevertheless, such modeling assumptions are not always justified; for example stochasticity plays a critical role for mobility, facilitating rolling [37], targeted arrest [40], or other walking modes [51]. Finally, a systematic derivation of macroscopic mobility from microscopic details that is valid under a broad range of parameters has not, to the best of our knowledge, been carried out.

Our aim in this paper is to introduce tools to systematically derive an analytic expression for the effective mobility of a nanocaterpillar – through the calculation of its diffusion coefficient – by coarse-graining over the microscopic details of its legs. We consider a nanocaterpillar in an overdamped system, moving in one horizontal direction parallel to a sticky surface, with legs that bind and unbind to it passively, so the system is reversible. Starting from a model that includes the detailed spatial fluctuations of the legs, we use homogenization techniques [22, 52, 53] to average over these fluctuations and obtain an analytic expression for the effective long-time diffusion coefficient D_{eff} of the particle (Sec. I.) This effective diffusion coefficient depends in a non-trivial way on the friction coefficients of the individual components of the system (legs and particle), with the frictions either adding up arithmetically (like springs in parallel) or harmonically (like springs in series) according to the mechanistic details. The effective diffusion can sometimes be orders of magnitude smaller than the background diffusion coefficient, showing the critical effect of the legs on the particle’s mobility.

We validate our analytic calculations with numerical simulations, which show the expression is accurate over a wide range of parameter values. We also conduct experiments with DNA-coated colloids, and show the measured diffusion coefficient agrees reasonably well with our model over a range of temperatures (Sec. II). This agreement was surprising to us, since our model does not yet capture two-dimensional modes of motion such as rolling, which are thought to lead to faster diffusion for DNA-coated colloids [33, 53]

Although our model is limited to motion in one dimension, we may still distinguish two long term modes

of motion: *sliding*, where at least one bond is always attached to the surface, and *hopping*, where the particle detaches completely, moves in free space and reattaches. These regimes are controlled by physical properties of the legs, such as stiffness and adhesive strength, and we classify existing biological and biomimetic systems in a so-called Ashby chart for nanocaterpillars (Sec. III).

Finally, we derive the effective diffusion coefficient for several variations of the model with varying assumptions, and argue that our model is the most general: it incorporates the results of other studies as special limits [22, 53], but is accurate over a broader range of parameters and system designs (Sec. IV). Overall, our results lay the ground to tune mobility features in artificial designs, and provide methodological tools to study more complex motion mediated through ligand-receptors, including rolling or self-avoiding walks due to active cutting of bonds.

I. HOMOGENIZATION TO OBTAIN THE EFFECTIVE DIFFUSION COEFFICIENT

We first illustrate our homogenization technique by considering a 1-legged caterpillar, an example we flesh out in great detail, and then generalize these results to a N-legged caterpillar.

A. 1-legged caterpillar: constitutive equations

We begin with the simplest possible model: a nanocaterpillar with a single leg (Fig. 2). The leg is permanently fixed to the caterpillar while its other end is mobile, and can attach anywhere on the binding surface. We consider a one-dimensional model, where leg fluctuations and particle motion occur on a line, longitudinal to the surface.

The dynamics of the particle position $x(t)$ and leg length $l(t)$ occur over nano to microscales, mostly in dense fluids such as water. In this context, dynamics are well captured by overdamped Langevin equations [54], where inertia plays a negligible role. This is in contrast to previous modeling efforts which used the Langevin equation (with inertia) [53], a point we return to in Sec. IV.

When the legs are unbound they evolve as

$$\frac{dl}{dt} = -\frac{k}{\gamma}(l(t) - l_0) + \sqrt{\frac{k_B T}{\gamma}} \eta_l(t). \quad (1)$$

Here k is a spring constant describing the recall force of the leg material, γ is its friction coefficient, l_0 its rest length, k_B is Boltzmann’s constant, T is temperature and η_l is a Gaussian white noise satisfying $\overline{\eta_l(t)} = 0$ and $\overline{\eta_l(t)\eta_l(t')} = 2\delta(t-t')$ where $\bar{\cdot}$ is the average over realizations of the noise. In most systems we consider, legs are made of polymers or proteins, where small leg deformations around equilibrium are well captured by a constant spring constant k [55–57].

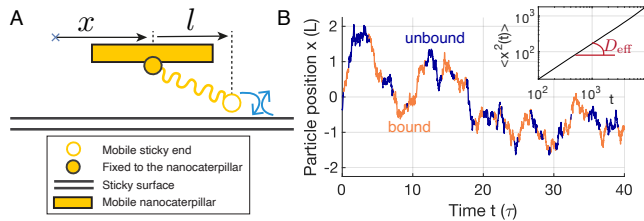


FIG. 2. **1D, 1-legged nanocaterpillar model.** (A) The longitudinal extension of the single leg (l) is monitored and feeds back into the longitudinal position (x) of the particle. (B) Simulation trace of the position of a 1-legged particle with time. (inset) The effective long time diffusion D_{eff} is half the slope of the mean squared displacement over long times.

The particle's position x when the leg is unbound obeys

$$\frac{dx}{dt} = \sqrt{\frac{k_B T}{\Gamma}} \eta_x(t) \quad (2)$$

where Γ is the friction coefficient of the particle and $\eta_x(t)$ is a Gaussian white noise uncorrelated with $\eta_l(t)$. The diffusion coefficient for the unbound particle is $D_0 = \frac{k_B T}{\Gamma}$. Note that this model for the simultaneous fluctuations of the particle + unbound leg is valid if the leg is fixed by its center of mass to the particle, with Γ representing $\Gamma' + \gamma$, the arithmetic sum of the bare particle friction Γ' and the leg friction γ (Supplementary 4.3). A model where the leg is not fixed by its center of mass results in minor modifications. Importantly, if the particle is 1-armed instead of 1-legged, with the fixed point on the surface (see Fig. 1-B) the equations presented here are exact. We ignore such details in the following and use 1-legged particles to account for particles with 1 adhesive point – discussing possible extensions in Sec. IV C.

We consider for now that the surface is uniformly coated with receptors. The leg can thus bind at any location on the surface. We introduce a constant binding rate to the surface q_{on} and constant unbinding rate q_{off} . Detailed balance requires $\frac{q_{\text{on}}}{q_{\text{off}}} = \frac{\pi_b}{\pi_u}$ where $\pi_{b/u}$ is the equilibrium probability of the system to be bound or unbound. Typically $\frac{\pi_b}{\pi_u} = e^{-\beta \Delta G}$, where $\beta^{-1} = k_B T$ and $\Delta G < 0$ is the free energy change when the leg binds to the surface [38, 58].

We now seek to describe motion of the system when the leg is bound. In this case, variables are constrained as $x(t) + l(t) - x_r = 0$ where x_r is the location of the receptor where the leg tip attached, which is constant until the leg detaches and reattaches to another location. The stochastic dynamics Eqs. (1) and (2) must be projected [32, 59] onto the constraint surface, see Appendix A. We obtain

$$\frac{dx}{dt} = -\frac{dl}{dt} = \frac{k}{\Gamma + \gamma} (l(t) - l_0) + \sqrt{\frac{k_B T}{\Gamma + \gamma}} \eta(t) \quad (3)$$

where $\eta(t)$ is a Gaussian white noise. Here we see that the projected dynamics have a natural expression where

the effective friction in the bound state is the arithmetic sum of the friction coefficients in the unbound states, $\Gamma + \gamma$. Note that this projection is a crucial step that is often ignored in such derivations [22, 32, 53], and modifies the dynamics in non trivial ways especially with a large number of legs.

The dynamics are now specified through the set of Eqs. (1)-(3), together with the binding and unbinding dynamics. To see what happens over long times, we simulate trajectories for 1 leg – see Fig. 2-B (and simulation details in Appendix A.2). Over long times, the particle's mean-squared displacement grows linearly with time, and we may extract an effective long time diffusion coefficient D_{eff} – see inset of Fig. 2-B. The computational cost of these simulations is high, since small time steps are required to resolve the fast relaxation and binding events. We therefore seek an analytic method to coarse-grain over these fast timescales.

B. Homogenization to coarse-grain the fast dynamics

1. Set up: partial differential equations to be coarse-grained

The set of stochastic Eqs. (1)-(3) defines a Markov process that is conveniently studied via the Fokker-Planck equation and its adjoint, the Kolmogorov backward equation [52, 60]. Let $p(x, l, t) = (p_u(x, l, t), p_b(x, l, t))$ be the probability density function of finding the system at time t and position x, l in the unbound or bound states. We obtain from Eqs. (1)-(3) the Fokker-Planck equation

$$\partial_t p = \mathcal{L}^* p, \quad (4)$$

with $\mathcal{L}^* = \mathcal{V}^* + \mathcal{Q}^*$ where

$$\mathcal{V}^* = \text{diag} \left(\begin{array}{c} \partial_l \left(\frac{k}{\gamma} (l - l_0) + \frac{k_B T}{\gamma} \partial_l \right) + \frac{k_B T}{\Gamma} \partial_{xx} \\ (\partial_l - \partial_x) \left(\frac{k}{\Gamma + \gamma} (l - l_0) + \frac{k_B T}{\Gamma + \gamma} (\partial_l - \partial_x) \right) \end{array} \right),$$

$$\mathcal{Q}^* = \begin{pmatrix} -q_{\text{on}} & q_{\text{off}} \\ q_{\text{on}} & -q_{\text{off}} \end{pmatrix},$$

with an appropriate initial condition. Additionally we require the flux in either state to vanish at infinity, to conserve total probability. The stationary solution of Eq. (4) is $\pi = \begin{pmatrix} q_{\text{off}} \\ q_{\text{on}} \end{pmatrix} \frac{e^{-\beta k (l - l_0)^2}}{Z}$ where Z is a normalization constant. This is therefore the equilibrium probability density of the system; one can verify that it satisfies detailed balance.

While probability densities have an intuitive physical meaning, in the following it will be easier – and mathematically better posed – to consider the adjoint of the Fokker-Planck equation and the corresponding dual functions. These are functions $f(x, l, t) = \int p(x', l', t | x, l) g(x', l') dl' dx'$ that give the expectation of any scalar function $g(x(t), l(t))$, given an initial condition

$x(0) = x, l(0) = l$. Once we know how such functions f evolve, we may calculate any statistic g of our stochastic process at any time, and hence the dynamics of f fully specify the dynamics of our process.

Writing $f(x, l, t) = \begin{pmatrix} f_u(x, l, t) \\ f_b(x, l, t) \end{pmatrix}$, we have that f satisfies the Kolmogorov backward equation [60]

$$\partial_t f = \mathcal{L}f, \quad f(x, l, 0) = g(x, l). \quad (5)$$

Here \mathcal{L} is the adjoint operator of \mathcal{L}^* , defined by the operator that satisfies $\langle f, \mathcal{L}^*p \rangle = \langle \mathcal{L}f, p \rangle$ for any probability density p and statistic f , where $\langle f, p \rangle = \iint (f_u p_u + f_b p_b) dl dx$ is the inner product.

2. Non-dimensionalization and assumptions on scales.

We now seek to coarse-grain the fast dynamics, by applying homogenization techniques to the backward equation, Eq. (5). To start, we nondimensionalize the equation using

$$x \rightarrow L_x \tilde{x}, \quad l - l_0 \rightarrow L \tilde{l}, \quad t \rightarrow \tau \tilde{t}, \quad (6)$$

where $L = \sqrt{k_B T/k}$ is the reference length of the leg fluctuations, L_x is the scale for the long-time average motion of x , and τ is the timescale associated with this average motion. The latter two scales are not determined *a priori* by any intrinsic scales in the system, but rather are chosen large enough that averaging will be appropriate over such scales; hence we choose $L_x = L/\epsilon$ where $\epsilon \ll 1$ is a small nondimensional number. We are interested in long time scales corresponding to the diffusion of the particle, hence we expect $\tau = L_x^2/D_0$, which corresponds to $\tau = \frac{1}{\epsilon^2} \frac{\Gamma}{k}$. Importantly, and in contrast with other works [22, 50], here ϵ does not measure the value of physical parameters, but rather, it measures the large observation time scale over which the coarse-grained model is valid. Such long observation times are quite likely in experiments, as typical binding rates and leg dynamics occur at most over 1 ms–1 s while observation (or other biophysical processes such as internalisation for viruses [17]) happens over the course of 10 min at least [38].

We now assume that the observation time scale is long enough, such that binding and unbinding events, as well as relaxation dynamics, will both occur on comparably short time scales. We can therefore write $\tilde{q}_i = q_i \Gamma/k = O_\epsilon(1)$ and $\gamma/\Gamma = O_\epsilon(1)$. In Sec. IV we will see that taking different limits for these physical parameters (such as $\gamma/\Gamma \ll 1$) yields the same result as applying these limits to the final result. Our choices of scalings are therefore quite general and can be easily adapted to more detailed systems.

Using nondimensional variables (and dropping the $\tilde{\cdot}$ for simplicity) we obtain from the backward equation Eq. (5) a separation in orders of ϵ as

$$\partial_t f = \mathcal{L}f = \left(\frac{1}{\epsilon^2} \mathcal{L}_0 + \frac{1}{\epsilon} \mathcal{L}_1 + \mathcal{L}_2 \right) f \quad (7)$$

where

$$\begin{aligned} \mathcal{L}_0 &= \begin{pmatrix} -q_{\text{on}} + \frac{\Gamma}{\gamma}(-l\partial_l + \partial_l) & \\ & -q_{\text{off}} + \frac{\Gamma}{\Gamma+\gamma}(-l\partial_l + \partial_l) \end{pmatrix}, \\ \mathcal{L}_1 &= \text{diag} \left(0, \frac{\Gamma}{\Gamma+\gamma} (l\partial_x - 2\partial_x) \right), \\ \mathcal{L}_2 &= \text{diag} \left(\partial_{xx}, \frac{\Gamma}{\Gamma+\gamma} \partial_{xx} \right). \end{aligned}$$

3. Homogenization method.

We seek a solution to Eq. (7) of the form $f = f_0 + \epsilon f_1 + \epsilon^2 f_2 + \dots$. We obtain a hierarchy of equations at different orders in ϵ :

$$O_\epsilon \left(\frac{1}{\epsilon^2} \right) : \quad \mathcal{L}_0 f_0 = 0, \quad (8)$$

$$O_\epsilon \left(\frac{1}{\epsilon} \right) : \quad \mathcal{L}_0 f_1 = -\mathcal{L}_1 f_0, \quad (9)$$

$$O_\epsilon(1) : \quad \mathcal{L}_0 f_2 = \partial_t f_0 - \mathcal{L}_1 f_1 - \mathcal{L}_2 f_0, \quad (10)$$

$$\vdots \quad \quad \quad \vdots$$

and we solve these iteratively for f at each order in ϵ . At lowest order we obtain from Eq. (8) and the vanishing flux at boundaries, $f_0 = a(x, t) \begin{pmatrix} 1 \\ 1 \end{pmatrix}$, where $a(x, t)$ is an unknown function of the slow variable x , whose dynamics we seek to determine. The associated equilibrium distribution at lowest order, $\mathcal{L}_0^* \pi_0 = 0$ is simply the full one $\pi_0 = \pi$.

At the next order, one can check that

$$f_1 = \left(\frac{\gamma q_{\text{on}}}{\Gamma + \gamma q_{\text{on}}} \right) \frac{l \partial_x a}{\Gamma(1 + q_{\text{off}}) + \gamma(q_{\text{on}} + q_{\text{off}})} \quad (11)$$

is a particular integral of Eq. (9), and is the unique solution since we impose that f_1 does not contain terms in the nullspace of \mathcal{L}_0 .

Finally Eq. (11) possesses a solution if and only if it satisfies the Fredholm alternative [52]

$$\langle (\partial_t f_0 - \mathcal{L}_1 f_1 - \mathcal{L}_2 f_0), \pi_0 \rangle = 0. \quad (12)$$

Standard algebra yields an effective long time diffusion equation for a (in dimensional variables)

$$\partial_t a = \frac{k_B T}{\Gamma_{\text{eff}}} \partial_{xx} a, \quad (13)$$

where

$$\begin{aligned} \frac{1}{\Gamma_{\text{eff}}} &= \frac{p_0}{\Gamma_0} + \frac{p_1}{\Gamma_1}, \quad \text{with } \Gamma_0 = \Gamma, \quad \Gamma_1 = \Gamma + \gamma_{\text{eff}} \\ \text{and } \gamma_{\text{eff}} &= \gamma + k \left(\frac{1}{q_{\text{off}}} + \frac{\gamma q_{\text{on}}}{k q_{\text{off}}} \right). \end{aligned} \quad (14)$$

In the above expressions, $p_0 = \frac{q_{\text{off}}}{q_{\text{off}} + q_{\text{on}}}$ is the equilibrium probability to have no bond, and $p_1 = 1 - p_0$ the equilibrium probability to have one bond. $\Gamma_0 = \Gamma$ is the friction

in the unbound state and Γ_1 is the effective friction contributing to the bound state.

Eq. (13), which is the backward equation for the particle+leg over long times, is one of the main results of this paper. It is the backward equation for a particle that evolves as

$$\frac{dx}{dt} = \sqrt{\frac{k_B T}{\Gamma_{\text{eff}}}} \eta_x(t). \quad (15)$$

That is, the particle diffuses, with effective diffusion coefficient $D_{\text{eff}} = \frac{k_B T}{\Gamma_{\text{eff}}}$ where Γ_{eff} is given by Eq. (14). The effective diffusivity and friction have the usual interpretation. In particular, if a potential $\mathcal{U}(x)$ were added to the particle Eqns. (2) and (3), one would recover in Eq. (15), following the same coarse-graining procedure, a term $-\frac{1}{\Gamma_{\text{eff}}} \partial_x \mathcal{U}$.

In Fig. 3 we compare the analytic result obtained in Eq. (14) (gray line) to numerical simulations of the full stochastic Eqs. (1)-(3) (gray dots). We show the results for a number of system parameters and find perfect agreement over several orders of magnitude.

C. How microscopic parameters determine long term diffusion

How shall we interpret the expressions for the effective diffusivity and friction? The effective diffusivity is a weighted sum of the diffusivity in each state, $D_{\text{eff}} = p_0 D_0 + p_1 D_1$ where the weights correspond to the probability to be in either state, and $D_i = k_B T / \Gamma_i$. The effective friction, on the other hand, is a harmonic weighted sum of the friction coefficients. That the diffusivity averages arithmetically is to be expected, since the mean squared displacement is an extensive quantity in a system with multiple states. That is, over a time t we can write

$$\begin{aligned} \overline{x^2(t)} &= 2D_{\text{eff}}t = 2D_0 p_0 t + 2D_1 p_1 t \\ &= 2D_0 t_0 + 2D_1 t_1 = \overline{x^2(t)}|_0 + \overline{x^2(t)}|_1, \end{aligned}$$

where t_0 and t_1 refer to the time spent in either state. The novelty here is that the diffusivity in the bound state,

$$D_1 = k_B T (\Gamma + \gamma_{\text{eff}})^{-1} \neq k_B T (\Gamma + \gamma)^{-1},$$

is obtained not just from the friction in the bound state, see Eq. (14), but is modified by spring resistance during binding events by an additional term $\gamma_{\text{eff}} - \gamma$.

We can interpret this additional term by writing it as

$$\gamma_{\text{eff}} - \gamma = k\tau_{\text{eff}}, \quad \text{where } \tau_{\text{eff}} = \tau_b + \tau_u^{\text{relax}}$$

is the typical time over which the leg's spring resistance acts, with $\tau_b = 1/q_{\text{off}}$ representing the average bound time, and $\tau_u^{\text{relax}} = \frac{\gamma}{k} \frac{q_{\text{on}}}{q_{\text{off}}} = \frac{\gamma}{k} \frac{\tau_b}{\tau_u}$ representing the bare relaxation time γ/k increased by the ratio of average bound time to average unbound time. This is coherent as the leg

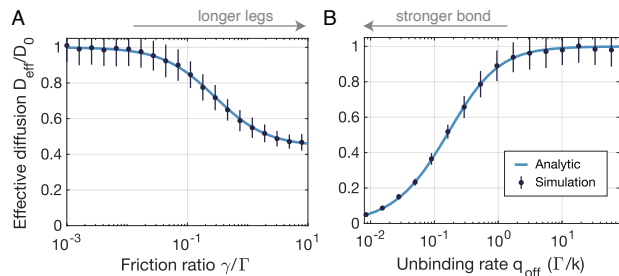


FIG. 3. **Effective diffusion D_{eff} of a 1-legged particle.** Simulation and analytic result Eq. (14) for a 1D system with 1 leg, with respect to (A) friction ratio γ/Γ and (B) unbinding rate q_{off} . (A) and (B) share the same y-axis. The other numerical parameters are $q_{\text{on}}\Gamma/k = 1.0$, and for (A) $q_{\text{on}}\Gamma/k = 0.8$ while for (B) $\gamma/\Gamma = 0.1$. Error bars represent one standard deviation for 100 independent runs.

fluctuations may only relax in the unbound state. The interpretation of τ_{eff} is comparable to that in Ref. [53].

Fig. 3 shows how the effective diffusion coefficient depends on microscopic parameters such as the leg friction and binding rates. As the leg friction γ increases, the effective diffusion of the particle decreases. When the leg friction γ is large compared to all other contributions to friction, diffusion in the bound state is frozen $D_1 = 0$, and the effective diffusion corresponds only to mobility in the unbound state $D_{\text{eff}} = p_0 D_0$ ($p_0 = 0.8/1.8 \simeq 0.44$ in Fig. 3-A). Leg friction is typically proportional to the size of the legs, and it is expected that the bigger the legs, the slower the particle. As the unbinding rate q_{off} decreases, D_{eff} decreases to arbitrarily small values. This slow down is due to spring recall forces acting over longer times until the particle freezes in a given location. Note that similar dependencies of the diffusion coefficient on the unbinding rate ($D_{\text{eff}} \sim k_B T q_{\text{off}}/k$) were noted in a numerical model of multivalent transport on discrete sites [44], in a theoretical investigation of sticky reptation in polymers [61], and were qualitatively observed experimentally in Influenza A viruses [19].

As a test of modeling choice, the analytic expression may also be plotted against numerical simulations of the non-dimensional equations with any value of ϵ . We find perfect agreement up to $\epsilon \lesssim 10$ (Supplementary Fig. S1), regardless of the choice of physical parameters. This highlights that the natural choice $\epsilon = L/L_x$ for coarse-graining purposes, corresponding to bound leg length scales versus unbound particle long range motion, is especially well suited for these types of problems. In the following ϵ is not incorporated in numerical simulations.

D. Effective diffusion with N legs

We extend our framework to probe nanocaterpillar dynamics with an arbitrary number of legs N (see Fig. 4-A). Eq. (1) is repeated for each unbound leg, and each leg binds to the surface with rates $q_{\text{on}}, q_{\text{off}}$ independently.

Eq. (2) gives the particle dynamics when no legs are bound. When n legs are bound, indexed by $i = 1, \dots, n$, the dynamics of the particle and bound legs are (Supplementary 1.2)

$$\frac{dx}{dt} = -\frac{dl_i}{dt} = \frac{k}{\Gamma + n\gamma} \sum_{i=1}^n (l_i - l_0) + \sqrt{\frac{k_B T}{\Gamma + n\gamma}} \eta. \quad (16)$$

The set of stochastic equations is now fully determined and can be simulated for any N , see Fig. 4-B.

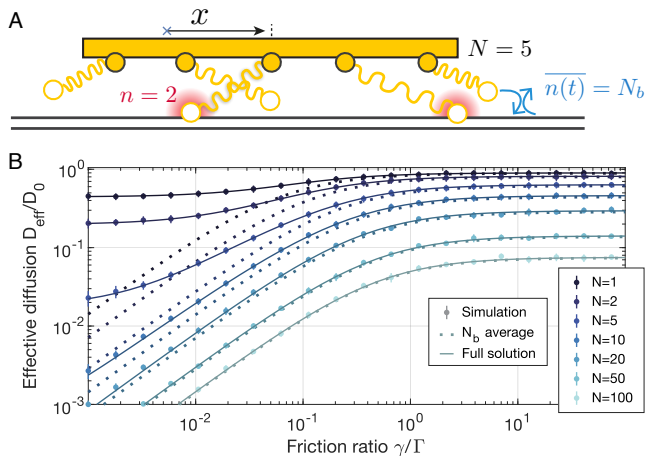


FIG. 4. **1D, N -legged nanocaterpillar model.** (A) The longitudinal extension of N legs are monitored (here $N = 5$) with binding and unbinding. The number of bonds $n(t)$ changes in time, here $n(t) = 2$. The average number of bonds is $\overline{n(t)} = N_b$ and depends on the binding and unbinding rates. (B) Simulations and analytic results for N -legs. “ N_b average” corresponds to Eq. (18) and “full solution” to Eq. (17). The other numerical parameters are $q_{on}\Gamma/k = 1.0$ and $q_{off}\Gamma/k = 0.8$.

Similarly as in Sec. IB, coarse-graining predicts a long time effective friction with N legs as (Supplementary 1.2)

$$\frac{1}{\Gamma_{\text{eff}}^{N \text{ legs}}} = \sum_{n=0}^N \frac{p_n}{\Gamma_n} \quad (17)$$

where $p_n = \binom{N}{n} \frac{q_{off}^{N-n} q_{on}^n}{(q_{off} + q_{on})^N}$ is the equilibrium probability to have n bonds and Γ_n is the friction coefficient in a state with n bonds. The frictions $\{\Gamma_n\}$ solve a linear system of equations that does not have a simple analytic solution, but can be solved using numerical linear algebra for given parameters as reported in Supplementary 1.2. We compare the numerically solved Eq. (17) (full lines) to numerical stochastic simulations with N legs (dots) in Fig. 4-B and find excellent agreement.

The coefficients Γ_n contributing to each bound state can be further investigated to yield an analytic approximation for $\Gamma_{\text{eff}}^{N \text{ legs}}$. When a large number of legs N is involved in the process, the dominant term in the sum of Eq. (17) corresponds to the average number of bonds

$N_b = \sum_{n=0}^N n p_n = \frac{q_{on}}{q_{off} + q_{on}} N$. Furthermore, one expects that the coefficients vary weakly around $n = N_b$, simplifying the linear system for the $\{\Gamma_n\}$, yielding

$$\frac{1}{\Gamma_{\text{eff}}^{N \text{ legs}}} \underset{N \gg 1}{\approx} \frac{1}{\Gamma_{N_b}} = \frac{1}{\Gamma + N_b \gamma_{\text{eff}}}. \quad (18)$$

The right hand side of Eq. (18) is valid regardless of parameter values (Fig. S4) and provides a good approximation for $\Gamma_{\text{eff}}^{N \text{ legs}}$ for large values of N (Fig. S3). For example, close agreement with Eq. (17) is obtained as early as $N = 20$, while good qualitative agreement is obtained for $N = 5$ (see Fig. 4-B, dotted line). Eq. (18) shows that the effective friction with N legs decays linearly with the *average* number of bonds N_b . For systems with a large number of legs (and hence potentially a large average number of bonds), we therefore expect a strong diffusion decrease due to enhanced friction with the surface.

II. EXPERIMENTAL MEASUREMENTS: DNA-COATED COLLOIDS DIFFUSING ON A DNA-COATED SURFACE

To probe the predicted strong decrease in diffusion with increasing numbers of bound legs, and to further validate our model, we conduct experiments with DNA-coated colloids, which provide a well-controlled model system for testing our analytic results. Such colloids bind and move relative to one another with complementary DNA strands acting as legs. The number of legs N in the contact region can exceed 100 [38, 62], suggesting they could cause a significant decrease in diffusion. The number of legs may be tuned by changing the temperature of the bath, as temperature controls the relative distance between surfaces [38].

A. Diffusion of DNA-coated colloids spans 2 orders of magnitude

We track the positions of about 500 DNA-coated colloids with dense coating (1 DNA per 11 nm²) diffusing on a DNA-coated substrate, at various temperatures (see preparation details in Appendix C. 1 and experimental setup in Appendix Fig. 9). At low temperatures all particles lie close to the binding surface, but when temperature increases beyond a narrow window around $T_m = 56.5^\circ\text{C}$ (see Fig. 5-A), they “melt”, and all lift-off from the surface (move beyond the depth of focus h_c).

The motion of the particles on the surface is diffusive over a 4°C window around the melting transition: $\langle x^2(t) \rangle \propto t^\alpha$ with $\alpha \simeq 1$, where \mathbf{x} is the position of each particle on the surface plane. Below $T_m - 2^\circ\text{C}$ the motion of particles is subdiffusive, $\alpha < 1$, and above $T_m + 2^\circ\text{C}$ particle motion is no longer confined to the plane. We therefore focus only on the temperature region

corresponding to diffusive motion. Over this range, effective diffusivity D_{eff} is obtained by fitting the ensemble-averaged mean-square displacement to the power law $\langle x^2(t) \rangle = 4D_{\text{eff}}t$ (see Fig. 5-C, and Appendix C. 2.). Importantly, we find that mobility depends strongly on temperature, decreasing by two orders of magnitude over the 4°C temperature window. We seek to relate these observations to our analytic theory for D_{eff} .

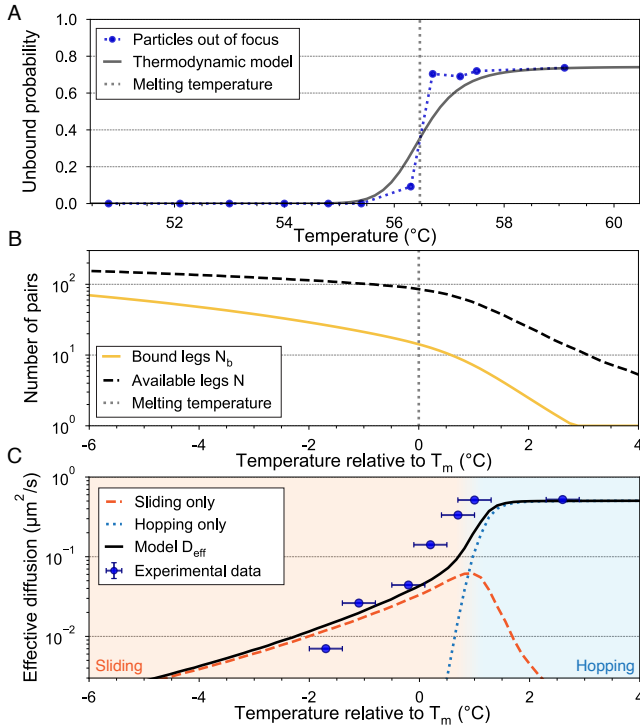


FIG. 5. **Mobility is controlled by temperature in DNA-coated colloids.** (A) Unbound probability for high coverage DNA-coated colloids measured near a surface and analytic prediction with 1 parameter fit (coating density of the substrate, obtained as $1/(10.8 \text{ nm}^2)$). (B) Number of available legs and average number of bound legs versus temperature, predicted by theory for the same system as in (A). (C) Diffusion coefficient of particles in (A) measured using particle tracking, and analytic prediction of effective diffusion coefficients (D_{eff} , D_{slide} , D_{hop}), computed respectively with Eqns. (17), (20) and (19) using N_b and N from (B). All calculated diffusion coefficients include corrections to account for the average height of the colloids with respect to the surface, obtained using vertical jumping rates Q_{on} and Q_{off} (see Appendix C.3 and Supplementary 2).

B. Number of legs controls the DNA-coated colloid diffusion

To evaluate D_{eff} from Eq. (17), we must evaluate the parameters of the 1D nanocaterpillar model. Some parameters (Γ , γ , k , q_{on} and q_{off}) are easily estimated using standard results for hydrodynamic friction, polymer dy-

namics [55], and adhesive dynamics [63] – see Table II. Other parameters, such as N and N_b (or equivalently N and the ratio $q_{\text{on}}/q_{\text{off}}$) require more extensive modeling of the detailed leg-arm interactions [38].

We thus calculate the detailed DNA-DNA brush interactions, accounting for leg density, leg length and DNA sequence, by evaluating the interaction energy $\phi(h)$ of the DNA-coated colloid with the surface. Following Ref. [38], $\phi(h)$ includes repulsive steric interactions [64] and attractive binding interactions, with entropic terms due to loss of degrees of freedom upon binding and competition for binding partners [58]. The unbound probability is obtained from the Boltzmann distribution as $p_u \sim \int_0^{h_c} e^{-\beta\phi(h)} dh$. With one fitting parameter, the coating density of the bottom substrate – the only parameter not accessible experimentally – we find predictions of the unbound probability that agree well with experimental data (see Fig. 5-A). The obtained value of the fitted parameter (1 DNA per 116 nm^2) is within the range of expected values (in particular, lower densities are expected on the flat surface compared to that on the particle [38]). The experimental melting transition is somewhat sharper than the predicted one, potentially due to softer brush tips than captured in the interaction model as shown in Ref. [38].

The average number of bonds N_b (gold in Fig. 5-B) and the number of legs within reach N (dashed black) with respect to temperature are then readily evaluated from the model leading to $\phi(h)$. The number of bonds at the melting temperature is only $N_b(T_m) \simeq 10$ while the number of available legs is quite high $N(T_m) \simeq 100$, stabilizing the interaction. The number of bonds N_b increases strongly with decreasing temperature, from 0 to 40 over the 4°C window, thus potentially accounting for most of the decrease in diffusion.

The effective diffusivity D_{eff} may then be evaluated using Eq. (17), see Fig. 5-C (black line). Since measurements includes colloid vertical motion beyond the binding range [65], we further include vertical motion and hence particle buoyancy through a $2 \times 1\text{D}$ model (see Appendix C.3). Such vertical motion is generally slow and only affects the effective probabilities p_n , not the friction coefficients Γ_n . The calculated values are in good agreement with experimentally measured diffusion coefficients near and slightly below T_m , with no fitting parameters (except the single parameter used to calibrate the model for the interaction energy $\phi(h)$). Above T_m , the experimentally measured diffusivity increases more sharply than the model’s prediction, though it stays within an order of magnitude.

This faster increase could be due to various factors; one possibility is the polymer brush is softer than modelled [38]. Another is the particles may move by rolling instead of by sliding [31], a motion which may have higher mobility at these temperatures [53]. In the opposite direction, at lower temperatures, subdiffusion occurs [31, 39], potentially due to inhomogeneities in the coated surfaces [31, 39, 42]. Such spatial dependencies

are not accounted for in our model but could be studied through spatially dependent attachment rates $q_{\text{on}}(x)$ or leg number $N(x)$. Nevertheless, although our one-dimensional model lacks these more complex ingredients and geometries, it predicts the hindered diffusion of DNA-coated colloids on surfaces near the melting temperature within an order of magnitude, and it explains why this diffusion changes so rapidly with temperature.

III. DO NANOCATERPILLARS SLIDE OR HOP?

Beyond quantitatively predicting effective diffusion, our model also gives insight into how particles move on the surface. For example, in our experiments, we can see colloids diffusing cohesively on the surface, except slightly above the melting temperature where colloids lift-off for short times and return to the surface. Previous experiments with lower leg densities observed colloids diffusing through a succession of uncohesive moves, namely hops above the surface [39]. The difference between cohesive and uncohesive modes of motion has been noted in a variety of other systems, ranging from virus mobility on surfaces [17, 19] to sticky polymer reptation [61]. We use our model to elucidate how a diversity of nanocaterpillars move in one-dimension – do they prefer to do so by “sliding” along the surface, or by “hopping” along it (see Fig. 6-A)?

A. What are sliding and hopping?

The mean squared displacement of a particle whose diffusion coefficient is determined from Eq. (17) can be split into two contributions, as

$$\begin{aligned} \langle x^2 \rangle &= 2D_{\text{eff}}t = 2p_0 \frac{k_B T}{\Gamma_0} t + 2 \sum_{n=1}^N p_n \frac{k_B T}{\Gamma_n} t \\ &\equiv 2D_{\text{hop}}t + 2D_{\text{slide}}t. \end{aligned}$$

We identify (a) a *hopping* mode (in accordance with Refs. [34, 39]) where the particle detaches *all bonds* with the surface and moves in free space (see Fig. 6-A), until it forms another bond. In this hopping mode

$$D_{\text{hop}} = p_0 \frac{k_B T}{\Gamma} = \left(\frac{q_{\text{off}}}{q_{\text{off}} + q_{\text{on}}} \right)^N \frac{k_B T}{\Gamma}. \quad (19)$$

We also isolate (b) a *sliding* mode (see Fig. 6-A) where the particle keeps at least one bond with the surface, a form of walking with no preferred direction,

$$D_{\text{slide}} = \sum_{n=1}^N \frac{p_n}{\Gamma_n} \simeq \frac{k_B T}{\Gamma_{N_b}} = \frac{k_B T}{\Gamma + N \frac{q_{\text{on}}}{q_{\text{off}} + q_{\text{on}}} \gamma_{\text{eff}}}. \quad (20)$$

The total mean-squared displacement can be broken up into the sum of the mean-squared displacement when

hopping, and the mean-squared displacement when sliding, as $\langle x^2 \rangle = 2D_{\text{hop}}t + 2D_{\text{slide}}t = \langle x^2 \rangle_{\text{hop}} + \langle x^2 \rangle_{\text{slide}}$.

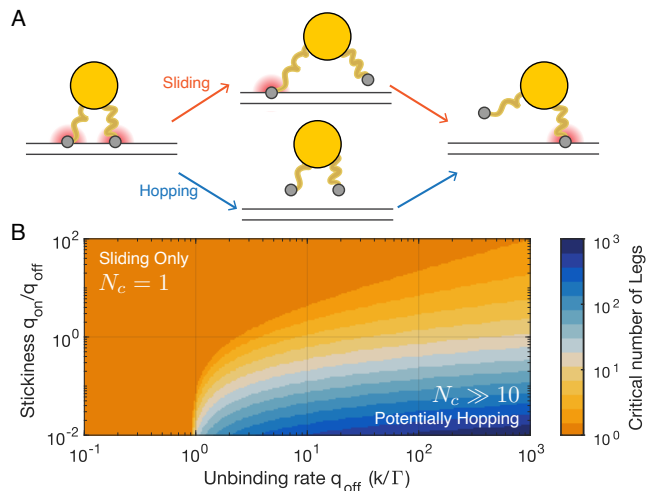


FIG. 6. **Nanocaterpillar diffusion modes with N legs.** (A) Typical modes of motion with N bonds: the nanocaterpillar may either slide (at least one bond remains attached to the surface) or hop (all bonds detach for the particle to move). (B) Critical number of legs N_c required for sliding to be more effective than hopping as a function of stickiness $q_{\text{on}}/q_{\text{off}}$ and unbinding rate.

Notice that D_{slide} decays with number of legs roughly as $1/N$, while D_{hop} decays exponentially with N , which is much faster. As soon as a few legs are involved, we may therefore expect that *sliding* dominates *hopping*. This interpretation is natural, since when a system has just a few legs ($N \simeq 1 - 2$), the odds that the legs all *detach* *once* are quite high, therefore favoring hopping. In contrast, in a system with a large number of legs, the odds that all legs *simultaneously* detach are simply too small, and the system walks randomly, remaining close to the surface. In a sense, nanocaterpillars truly are caterpillars walking with nanoscale legs.

In general, the critical number of legs $N_c(q_{\text{on}}, q_{\text{off}}, k, \gamma, \Gamma)$ required to favor sliding ($N \geq N_c$) over hopping ($N \leq N_c$) satisfies

$$\frac{\langle x^2 \rangle_{\text{slide}}}{\langle x^2 \rangle_{\text{hop}}} = \frac{D_{\text{slide}}}{D_{\text{hop}}} = 1 = \frac{\left(\frac{q_{\text{off}}}{q_{\text{off}} + q_{\text{on}}} \right)^{N_c}}{1 + N_c \frac{q_{\text{on}}}{q_{\text{off}} + q_{\text{on}}} \frac{\gamma_{\text{eff}}}{\Gamma}}. \quad (21)$$

The critical number of legs is controlled by the ratio $q_{\text{on}}/q_{\text{off}}$, termed henceforth *stickiness*, and by the magnitude of the effective friction in the bound states γ_{eff} , itself dominated in most systems by the unbinding rate q_{off} . We can therefore investigate N_c as a function of stickiness $q_{\text{on}}/q_{\text{off}}$ and unbinding rate q_{off} (Fig. 6-B). Overall, a system with say $N = 10$ legs is typically dominated by sliding motion. Yet hopping may still occur *e.g.* with large unbinding rate q_{off} . In fact q_{off} increases the friction γ_{eff} in the bound states and reduces D_{slide} .

B. Classifying biophysical systems

We now classify a diversity of biological and biomimetic systems within the framework of our model, and ask whether each tends to prefer sliding or hopping. Our model relies on 6 physical parameters $k, \gamma, q_{\text{off}}, q_{\text{on}}, \Gamma, N$ that can be estimated from the literature for many systems: viruses, molecular motors, white blood cells, protein cargos in the nuclear pore complex, bacteria such as *Escherichia coli*, and DNA-coated colloids (Supplementary 3).

Typically, stickiness values are similar across systems with $q_{\text{on}}/q_{\text{off}} \sim 0.05 - 0.8 \geq 1$ – except when the system is thermally manipulated, which is only the case in artificial designs, see Sec. II A. Therefore we consider $q_{\text{on}}/q_{\text{off}} \simeq 0.1$. Additionally, as legs are generally small compared to particles, $\gamma/\Gamma \simeq 10^{-3} - 10^{-1}$ and therefore the dominant factor in $\gamma_{\text{eff}}/\Gamma$ is usually controlled by spring recall force and unbinding times, as $k/\Gamma q_{\text{off}}$. We find $k/\Gamma q_{\text{off}} \simeq 10^{-2} - 10^8$ in the range of systems studied, confirming that this is a critical factor to discriminate nanocaterpillars. Additionally, as systems have a varied number of available legs for binding N , we define an effective relaxation rate

$$\frac{k^{(N)}}{\Gamma} = \frac{k}{\Gamma} N \frac{q_{\text{on}}}{q_{\text{off}} + q_{\text{on}}} \left[\left(\frac{q_{\text{off}} + q_{\text{on}}}{q_{\text{on}}} \right)^N - 1 \right]$$

that will allow us to predict either sliding or hopping.

We sort systems in a so-to-speak *Ashby* chart, according to the effective relaxation rate $k^{(N)}/\Gamma$ and detachment rate q_{off} (Fig. 7). This chart summarizes parameter ranges for different systems, and predicts which systems move by sliding and which move by hopping, at least when considering translational motion in one dimension. If $k^{(N)}/\Gamma q_{\text{off}} \leq 1$, according to Eq. (21), sliding (orange region) is favored over hopping (blue region). Different groups of systems emerge from this classification, that we review below.

1. Sticky hoppers

We predict that viruses, white blood cells, and molecular motors cannot slide. These systems show very long bond lifetimes, with $\tau_{\text{off}} = q_{\text{off}}^{-1} \simeq 1 - 100$ s. This is characteristic of strong bonds, for which the interaction energy $|\Delta G| \gg k_B T$. Since for the protein ligands in these systems, $k \simeq 10^{-4}$ N/m and $\Gamma \simeq 10^{-9}$ N.s/m for $1 \mu\text{m}$ particles, we expect $k/\Gamma \simeq 10^5 \gg q_{\text{off}}$ and therefore $\gamma_{\text{eff}} \gg \Gamma$. Therefore such systems simply can not slide. Sliding is even more disfavored for coronaviruses (Sars CoV 1 and 2), since the legs are made of very rigid proteins, with $k \simeq 0.5$ N/m [66, 67]. Hopping is therefore a probable mode of motion for these systems.

These predictions are qualitatively consistent with experimental measurements. The diffusion coefficient of an

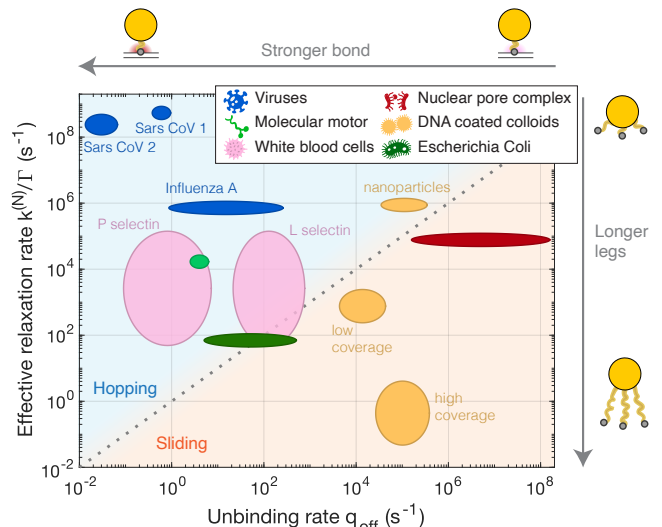


FIG. 7. **Sorting biophysical systems.** Expected regimes of sliding or hopping, according to the effective relaxation rate $k^{(N)}/\Gamma$ and unbinding rate q_{off} . The gray line corresponds to $k^{(N)}/\Gamma = q_{\text{off}}$ and separates sliding and hopping regions. Circles represent the range of values found in the literature for parameters of each system. Systems are color coded according to their category in the legend. When multiple systems belong to a category, details are indicated next to the circles. Low and high coverage DNA-coated colloids refer to $1 \mu\text{m}$ size colloids and nanoparticles to 15 nm size.

influenza A virus on protein-coated surfaces was measured as $D_0/D_{\text{eff}} \simeq 4 - 190$ [17, 19]. Although the virus particles in these experiments were more complex than our model, including *e.g.* cleaving bonds, and possibly mobile receptors, we may nevertheless compare the measurements to the model's predictions. Estimating the typical number of available legs $N \simeq 10$ [68, 69] and the bound probability $q_{\text{on}}/(q_{\text{on}} + q_{\text{off}}) = 20\%$ [69] yields $D_0/D_{\text{hop}} = [q_{\text{off}}/(q_{\text{on}} + q_{\text{off}})]^N \simeq 10$, in the range of measured values. Our model predicts that hopping is therefore more probable than sliding for influenza A. This is consistent with Ref. [17], which observed infrequent yet very long spatial steps, termed *gliding* moves. The influenza A virus may also move via cohesive short spatial steps, that have been attributed to rolling motion [5, 17, 19, 41]. Rolling is not accessible as part of our model, and may be due in this context to active bond cleaving [17, 19, 41] that is beyond the scope of passive binding as presented here. However, this serves as a reminder that other modes of motion may be observed for these systems, especially when they are out-of-equilibrium.

2. Slippery sliders

Reciprocally, we predict that systems with weak adhesion (equivalent to short bond lifetimes, *i.e.* large

q_{off}) may move by sliding. Such systems include proteins translocating through the nuclear pore complex, or white blood cells adhering through L-selectin linkers, which are notably weaker than P-selectin [23]. Sliding may also be accessible to systems with short effective relaxation rate, for which the sticky friction mediated by k/Γ is low. This corresponds to large particles with long legs, as is the case for Escherichia Coli [56] (dark green).

3. DNA-coated colloids

DNA-coated colloids at their melting temperatures span the nanocaterpillar chart (Fig. 7), with some sliding and some hopping depending on the size of the particle and the coating density. While the binding kinetics are roughly independent of particle size, the effective relaxation rate can vary strongly. Nanometre-sized colloids have fast relaxation rates as they are small (and therefore Γ is smaller), and are thus sticky hoppers. In contrast, large colloids have slower relaxation rates $k^{(N)}/\Gamma$, all the more as usually a great number of bonds $N \simeq 100$ are involved in the binding process, and thus are prone to slide.

The DNA coating density is also a significant factor. For DNA-coated colloids with low coverage densities, as in Ref. [39], the spacing between legs is too large and geometrically prevents sliding. Hence only hopping, or uncohesive motion with the surface, is observed, resulting in a much stronger slow down of diffusion with decreasing temperature [39]. Geometrical arguments yield $N \simeq 55$ available legs for binding with a bound probability $q_{\text{on}}/(q_{\text{on}} + q_{\text{off}}) \simeq 9\%$. Our model predicts $D_0/D_{\text{hop}} = [q_{\text{off}}/(q_{\text{on}} + q_{\text{off}})]^N \simeq 180$, which is in remarkable agreement with Ref. [39].

For DNA-coated colloids with dense coatings such as the ones synthesized here, we predict that sliding, or some form of cohesive motion with the surface, is usually the dominant motion mechanism. Indeed, we evaluated D_{hop} and D_{slide} from Eqns. (19) and (20) for our experimental system as a function of temperature (see Fig. 5-C). We find that, the high number of available legs, due to high coverage, prevents hopping around the melting temperature and that our colloids primarily slide, consistent with the observed cohesive motion. For example at the melting temperature, about $N \simeq 100$ legs are available, with stickiness $q_{\text{on}}/q_{\text{off}} \simeq 0.1$, giving $D_{\text{hop}}(T_m)/D_0 = [q_{\text{off}}/(q_{\text{on}} + q_{\text{off}})]^N \simeq 10^{-4}$, which is much slower than sliding. Hopping emerges as a favorable mode at 1°C above the melting point, where the average number of available and bound legs significantly decreases due to particle lift-off from the surface, a prediction that is again consistent with our qualitative observations. At these temperatures, the particles' motion is dominated by long excursions far from the surface. The transition occurs for a fairly small average number of bonds $N_b \simeq 5$, with about $N = 40$ legs in contact (see Fig. 5-B).

4. Design rules for sliding versus hopping

Herewith we can draw simple design rules for sliding or hopping. Numerous, long wobbly legs with weak adhesive bonds are well adapted for sliding. Short and stiff legs with strong adhesive bonds facilitate hopping. DNA-coated colloids offer various design features to control their mobility: for example, larger sizes, higher DNA coverage, and lower temperature all favor sliding. Further control can be achieved by tuning the microscopic features of the legs, such as their spring constants k , for example by choosing the length of the ligand leg [38]. However, it is especially hard to achieve experimentally *without* changing other experimental features at the same time. For example, current coating processes generally result in less dense coatings for longer legs [38].

Overall, these design rules thus allow to tune artificial systems for controlled mobility features. This could have consequences in particular in the field of self-assembly of artificial structures, where facilitated cohesive motion is believed to be essential for long-range alignment [31–33].

IV. COARSE-GRAINING UNDER DIFFERENT MODELS AND ASSUMPTIONS

In the physical and biological systems we explored, the range of physical parameters was quite broad, suggesting that other scaling ansätze might be appropriate to study the effective long term dynamics. In this section we review alternative approximations and compare them to the predictions of our model. To make the argument simpler, we mostly focus on a 1-legged caterpillar; the comparisons should be similar for a multi-legged caterpillar. Detailed coarse-graining steps using the different approximations described in this section are reported in Supplementary 4. All results are summarized in Table I and compared in Fig. 8.

A. Dynamics with inertia

One may include particle inertia with a small yet finite mass $m \neq 0$, by starting with the underdamped Langevin equations for the particle (rather than the overdamped Langevin equations as we have done) – see Ref. [53]. To understand the scales associated with mass, one can compare the correlation time of the particle's velocity when spring recall forces are at play, $\tau_v \simeq \frac{m(L_x/\tau)}{Lk}$, to the time scale of observation τ [53]. Coarse-grained dynamics require $\frac{\tau_v}{\tau} = \frac{mL_x}{Lk\tau^2} = O(\epsilon)$, which is apparently coherent with a small mass.

Coarse-graining steps (Supplementary 4.1) lead to an effective friction

$$\Gamma_{\text{eff}}^m = p_0\Gamma_0 + p_1\Gamma_1. \quad (22)$$

Notice that the effective friction is the arithmetic sum of the frictions in each state – not the harmonic sum ob-

Model	Sketch	Result
<i>Main geometries</i>		
1-arm		$\frac{1}{\Gamma_{\text{eff}}} = \frac{p_0}{\Gamma_0} + \frac{p_1}{\Gamma_1}, \Gamma_0 = \Gamma, \Gamma_1 = \Gamma + \gamma_{\text{eff}}, \gamma_{\text{eff}} = k \left(\frac{1}{q_{\text{off}}} + \frac{\gamma}{k} \frac{q_{\text{on}}}{q_{\text{off}}} \right)$
1-leg		$\frac{1}{\Gamma_{\text{eff}}} = \frac{p_0}{\Gamma_0} + \frac{p_1}{\Gamma_1}, \Gamma_0 = \tilde{\Gamma}, \Gamma_1 = \tilde{\Gamma} + \gamma_{\text{eff}}, \tilde{\Gamma} = \Gamma + \gamma^a$
N-legs		$\frac{1}{\Gamma_{\text{eff}}} = \sum_{n=1}^N \frac{p_n}{\Gamma_n}, p_n = \binom{N}{n} \frac{q_{\text{off}}^{N-n} q_{\text{on}}^n}{(q_{\text{off}} + q_{\text{on}})^N}, \Gamma_n = \Gamma + n\gamma_{\text{eff}}$
<i>Inertial dynamics</i>		
1-leg, inertia		$\Gamma_{\text{eff}} = p_0\Gamma_0 + p_1\Gamma_1, \Gamma_0 = \Gamma, \Gamma_1 = \Gamma + \gamma_{\text{eff}}$
<i>Limit regimes</i>		
Small legs		$\frac{1}{\Gamma_{\text{eff}}} = \frac{p_0}{\Gamma} + \frac{p_1}{\Gamma} \left(1 - \frac{\gamma_{\text{eff}}}{\Gamma} \right)$
Fast legs		$\frac{1}{\Gamma_{\text{eff}}} = \frac{p_0}{\Gamma_0} + \frac{p_1}{\Gamma_1}, \Gamma_0 = \Gamma, \Gamma_1 = \gamma + \frac{k}{q_{\text{off}}}$
Fast binding		$\frac{1}{\Gamma_{\text{eff}}} = \frac{p_0}{\Gamma_0} + \frac{p_1}{\Gamma_1}, \Gamma_0 = \Gamma, \Gamma_1 = \gamma + k \left(\frac{\gamma}{k} \frac{q_{\text{on}}}{q_{\text{off}}} \right)$
<i>Extended geometries</i>		
1-arm, 1-leg		$\frac{1}{\Gamma_{\text{eff}}} = \frac{p_0}{\Gamma_0} + \frac{p_1}{\Gamma_1}, \Gamma_0 = \Gamma, \Gamma_1 = \Gamma + \frac{1}{2}\gamma_{\text{eff}}$
M-arms, N-legs		$\left\{ \begin{array}{l} \frac{1}{\Gamma_{\text{eff}}} = \sum_{n=1}^N \frac{p_n}{\Gamma_n}, \Gamma_n = \Gamma + n\gamma_{\text{eff},n}(M, N), \\ (\gamma_{\text{eff},n}(M, N))^{-1} \simeq (\gamma_{\text{eff},M,n})^{-1} + (\gamma_{\text{eff},N,n})^{-1}, \gamma_{\text{eff},P,n} = \gamma + k \left(\frac{1}{q_{\text{off}}} + \frac{\gamma}{k} \frac{(P-n)q_{\text{on}}}{q_{\text{off}}} \right) \end{array} \right.$

^a if the leg's center of mass is fixed on the particle. In the following we ignore differences between Γ and $\tilde{\Gamma}$ to simplify notations.

TABLE I. Summary of different models and their effective long time friction.

tained in Eq. (14) [70]. Eq. (14) is equivalent to Eq. (22) in the limit where the friction correction is small, $\gamma_{\text{eff}} \ll \Gamma$ – see Fig. 8-B (yellow).

However, differences arise beyond this regime. For stiff legs ($\gamma/\Gamma \gg 1$, $k/q_{\text{off}}\Gamma \gg 1$) one finds $\Gamma_{\text{eff}}^m \sim 0$ while $\Gamma_{\text{eff}} \sim \Gamma$. This stark difference has an intuitive explanation: the particle may not move when it is attached with the stiff leg, but it can still move when it is unbound, and therefore the effective friction should remain finite. This is true *unless* the particle has significant inertia and therefore does not have the time to accelerate within the unbound periods. In fact, in the non-dimensionalization we implicitly assumed that $m/\Gamma = \epsilon L k \tau^2 / \Gamma L_x = \Gamma / k \epsilon^2$, such that the inertial relaxation time was in fact assumed to be large compared to the time scale of velocity fluctuations.

This drives the general question of how to account for inertia in such systems, and whether inertia plays a role in the macroscopic diffusion of nanocaterpillars. We will address this question thoroughly in another paper [71], in which we reconcile Eq. (22) and Eq. (14) through a model which includes inertia in all the degrees of freedom.

B. Choice of time-scale hierarchy

There are other choices for the ordering of time scales. We review these below: we describe their experimental relevance, then briefly examine the effective friction under these different approximations and compare it to our main result Eq. (14). We find that our choice of time-scale hierarchy is fairly general, as it encompasses other approximations as special limits of ours.

1. Fast leg dynamics compared to particle dynamics

One common approximation is to assume rapid leg dynamics compared to particle dynamics, with $\epsilon = \gamma/\Gamma$ [50]. Such an approximation is consistent with numerous experiments, as legs are typically short, hence fast because of Stokes relation, compared to the large particles investigated (such as white blood cells [7] or DNA-coated colloids [62]).

With this assumption one typically relaxes the restriction on lengthscales, as $L \sim L_x$. The observation time-scale is $\tau = L^2/D_0 = \Gamma/k$ and binding and unbinding are taken to be fast compared to this time scale,

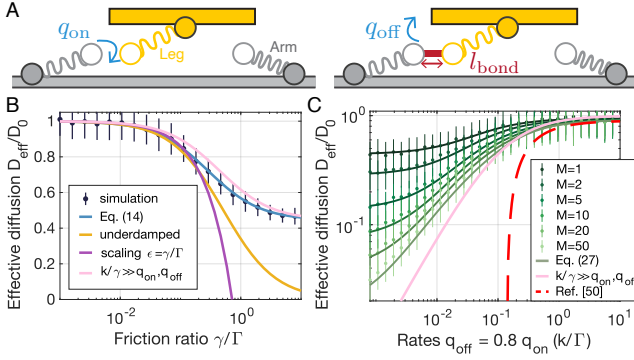


FIG. 8. **Comparing with other coarse-grained models and assumptions.** (A) Schematic for arm and leg dynamics considered in this work. (B) Effective diffusion with respect to friction ratio γ/Γ : calculated with Eq. (14), Eq. (22) (“underdamped”), and Eq. (23) (“scaling $\epsilon = \gamma/\Gamma$ ”). (C) Effective diffusion with respect to binding and unbinding rates (keeping q_{on}/q_{off} constant), for a particle with 1 leg facing $M = 1 - 50$ arms: calculated with Eq. (27), and Eq. (24) (“pre-averaging”, taking $p_0 = 0$ and $p_1 = 1$ to match the limit $M \rightarrow \infty$). Ref. [50] corresponds both to $k/\gamma \gg q_{on}, q_{off}$ and $\gamma/\Gamma = \epsilon$ and was plotted for consistency. For (A) and (B), shared numerical parameters are $q_{on}\Gamma/k = 1.0$, $q_{on}\Gamma/k = 0.8$ and $\gamma/\Gamma = 0.1$.

$q_{on} \sim q_{off} \sim 1/\tau\epsilon$. One obtains (Supplementary 4.2.1)

$$\frac{1}{\Gamma_{eff}^{\epsilon=\gamma/\Gamma}} = \frac{p_0}{\Gamma} + \frac{p_1}{\Gamma} \left(1 - \frac{\gamma_{eff}}{\Gamma}\right). \quad (23)$$

Eq. (23) results in a small correction to the effective friction, of order ϵ . It is equivalent to Eq. (14) in the limit where $\gamma_{eff} \ll \Gamma$ is small. The assumption $\epsilon = \gamma/\Gamma$ appears thus quite restrictive as it implicitly also requires to observe the system at long time scales compared to the other time scales in the system. Furthermore, contrary to Eq. (14) where the small parameter ϵ disappears, here $1/\Gamma_{eff}^{\epsilon=\gamma/\Gamma}$ is a first order expansion in $\epsilon \sim \gamma_{eff}/\Gamma$. We present Eq. (23) against Eq. (14) in Fig. 8-B (purple vs black) and find that Eq. (23) is indeed only valid for small values of γ/Γ . Our choice of scaling $\epsilon = L/L_x$ can thus account for a broad range of bare friction values.

2. Fast leg dynamics compared to binding dynamics

Another approximation assumes fast leg relaxation dynamics compared to binding dynamics, $k/\gamma \gg q_{on}, q_{off}$ (and both are fast compared to particle dynamics). In this case leg lengths are sampled from their equilibrium distribution when they bind, corresponding to a “pre-averaging” approximation. Leg lengths are not tracked when they are unbound, allowing to speed up simulations [22, 33, 50, 72]. This limit is relevant to describe stiff legs, *e.g.* rigid polymers such as double stranded DNA – see Table S1.

Coarse-graining gives (Supplementary 4.2.2)

$$\frac{1}{\Gamma_{eff}^{k/\gamma \gg q}} = \frac{p_0}{\Gamma} + \frac{p_1}{\Gamma + \gamma + \frac{k}{q_{off}}}. \quad (24)$$

How can we relate pre-averaging dynamics to our theory for a leg binding to uniformly sticky surface described in Sec. I? The pre-averaged result Eq. (24) is comparable to the coarse-grained result of Sec. I, Eq. (14), except for the relaxation term involving τ_u^{relax} in γ_{eff} , confirming that τ_u^{relax} originates from unbound relaxation dynamics. This difference results in some differences in D_{eff} , depending on the microscopic parameters (Fig. 8-B). Additionally, the pre-averaged limit may be viewed as the limit regime for a nanocaterpillar with a large number of legs, say $N \gg 1$, where on average 1 or 0 leg is bound to the surface, $N_b \lesssim 1$. This typically requires $q_{on} \ll q_{off} \ll k/\gamma$, and indeed Eq. (17) converges to the pre-averaged result in that limit (Supplementary Fig S4).

The validity of pre-averaging is limited to the domain $q_{on}, q_{off} \ll k/\gamma$. In systems such as DNA-coated colloids, binding rates q_{on} and q_{off} may be manipulated over orders of magnitude [73], by choosing the DNA sequence or by adjusting temperature, potentially accessing $q_{on} \gg q_{off} \gg k/\gamma$ at low temperatures. In this regime, Eq. (14) predicts that the nanocaterpillar is frozen in the bound state, while pre-averaged dynamics still predict a non zero mobility. In these situations pre-averaged dynamics are therefore not suitable. We show later however that introducing numerous arms – more generally a lot of binding partners – can extend the validity range of pre-averaging.

3. Fast binding dynamics compared to leg dynamics

Finally, one can consider fast binding dynamics compared to leg dynamics, $q_{on}, q_{off} \gg k/\gamma$. Although this limit is not often considered in simulations, it is relevant for dense arrangements of receptor sites [62]. In fact as the binding rate q_{on} scales linearly with the concentration of receptors, it can increase by orders of magnitude for a leg potentially in contact with a dense arm array – see Table S1.

Coarse-graining yields (Supplementary 4.2.3)

$$\frac{1}{\Gamma_{eff}^{q \text{ fast}}} = \frac{p_0}{\Gamma} + \frac{p_1}{\Gamma + \gamma + k \left(\frac{\gamma q_{on}}{k q_{off}}\right)} \quad (25)$$

which is exactly what is expected in the limit $q_{on}, q_{off} \gg k/\gamma$ in Eq. (14). Again, this highlights the physical mechanisms yielding the different contributions in γ_{eff} . Here the average bound time of the leg is small, $\tau_b \ll \gamma/k$, and therefore does not contribute to γ_{eff} .

C. Arms and/or legs

The diversity of nanocaterpillars resides also in their geometry: some particles have legs that attach to a surface [74], some have no legs (or infinitesimally small legs), with binding sites directly on the particle that attach to outstretched receptors on the surface that we refer to as arms [22, 50] (1 arm case in Tab. I) and some have both outstretched legs connecting to outstretched arms [33] (arms and legs in Tab. I).

1. Arms or legs

A particle with a leg or a bare particle attaching to an arm (1-legged and 1-armed respectively, see Tab. I) have nearly equivalent effective dynamics. The only difference resides in the interpretation of Γ in the unbound leg dynamics Eq. (2) – see Supplementary 4.3.1. For the 1-legged case, if the leg’s center of mass corresponds to the point grafted to the particle, the unbound friction coefficient is simply increased by the leg as $\Gamma \rightarrow \Gamma + \gamma$, where Γ is the bare particle friction coefficient and γ the leg’s. If the leg’s center of mass is offset from the grafting point on the surface, minor modifications have to be made to Eq. (2) yet lead to very similar dynamics overall – see Supplementary 4.3.1. For the 1-armed case, we simply have the unbound friction coefficient Γ to be the bare friction coefficient of the particle. This justifies our approach, where we ignore the details of the leg or arm location and simply treat them as mathematically equivalent.

2. Arm and leg

A 1-legged particle attaching to 1 arm has slightly more interesting dynamics. To investigate this case, we simplify the problem and consider that the leg can bind to the arm regardless of their relative location, with a rigid rod of length l_{bond} that bridges the gap between the sticky points (see Fig. 8-A). In the bound state the constraint is thus $x + l_{\text{leg}} - l_{\text{arm}} = l_{\text{bond}}$. The relative distance l_{bond} is unimportant and can be assumed to be zero, and therefore this model effectively creates an arm with the correct length each time the leg binds.

Although the model is simplistic, it is realistic in the presence of a dense periodic array of arms (where the leg can only bind to 1 arm at a time), and allows us to compare the mechanical properties of this geometry compared to a single leg or arm. We find using similar coarse-graining techniques (Supplementary 4.3.2)

$$\frac{1}{\Gamma_{\text{eff}}^{\text{leg+arm}}} = \frac{p_0}{\Gamma} + \frac{p_1}{\Gamma + \gamma_{\text{eff},1}(1,1)} \text{ where } \gamma_{\text{eff},1}(1,1) = \frac{\gamma_{\text{eff}}}{2}. \quad (26)$$

The added friction in the bound state is only half that with a single leg or a single arm. In fact, here friction

is distributed harmonically, like the effective spring constant of two springs in series. Note however that attaching springs with different spring constants would not lead to a similar harmonic sum of effective frictions, as the effective friction contains more contributions than those originating from the spring recall force (analytic results not shown here). Slightly improved mobility is therefore achieved with both an arm and a leg, while the qualitative behavior of the original model is preserved.

3. Leg facing numerous arms

We now consider a leg that can bind to *multiple* arms at the same time. As in the previous section, the arms do not have particular locations but rather appear with the correct lengths when needed. Following the formalism of arm and leg dynamics detailed above (Supplementary 4.3.3) one finds that with M arms,

$$\frac{1}{\Gamma_{\text{eff}}^{\text{leg+}M \text{ arms}}} = \frac{p_{M,0}}{\Gamma} + \frac{p_{M,1}}{\Gamma + \gamma_{\text{eff},1}(M,1)} \quad (27)$$

and $p_{M,0} = q_{\text{off}}/(q_{\text{off}} + Mq_{\text{on}})$ and $p_{M,1} = 1 - p_{M,0}$ are the probabilities to have 0 or 1 bond. The added friction $\gamma_{\text{eff},1}$ is a harmonic average when M is large

$$\frac{1}{\gamma_{\text{eff},1}(M,1)} \underset{M \gg 1}{\approx} \frac{1}{\gamma_{\text{eff},M,1}} + \frac{1}{\gamma_{\text{eff},1,1}}, \quad (28)$$

with $\gamma_{\text{eff},M,1} = k \left(\frac{1}{q_{\text{off}}} + \frac{\gamma}{k} \frac{(M-1)q_{\text{on}} + q_{\text{off}}}{q_{\text{off}}} \right)$ the effective friction due to the leg $\gamma_{\text{eff},1,1} = k \left(\frac{1}{q_{\text{off}}} + \frac{\gamma}{k} \right)$ due to arms. We see that the factors implying the unbound relaxation time $\tau_{\text{u}}^{\text{relax}}$ are modified in each case. We give the following interpretation: the average unbound time for the leg is $\tau_{\text{u}} = 1/(M-1)q_{\text{on}}$, due to $M-1$ other available arms to bind to. For the arms $\tau_{\text{u}} = \infty$ as there are no other legs to bind to once the only leg is bound. The harmonic average in Eq. (28) highlights again that the leg-arm configuration is mathematically similar to the effective force of springs in series.

In the limit of a large number of arms M , the leg is always bound to the surface ($p_1 = 1$) and the correction to the bound state friction converges to

$$\gamma_{\text{eff},1}(M,1) \xrightarrow{M \rightarrow \infty} \gamma_{\text{eff},1}(1,1) = \gamma + \frac{k}{q_{\text{off}}}, \quad (29)$$

which is the correction to the effective friction for the pre-averaging result, Eq (24).

This limit is surprising. Sec I, Eq. (14) showed that for a leg binding to a uniformly sticky surface, in the limit where the leg is always bound ($p_1 = 1$), the nanocaterpillar is frozen and $D_{\text{eff}} = 0$. When the leg is bound to a great many arms this is no longer the case: we recover the diffusion coefficient associated with preaveraging. We interpret this discrepancy as follows. With many arms binding to a leg, the particle may still move, even

in a parameter regime where the leg is effectively frozen, and relaxes to equilibrium on very long timescales. In fact, the leg swaps between different arms, which have different random lengths and hence apply different random forces, causing the particle’s position to fluctuate. Indeed, in Eq. (29) it is apparent that the remaining friction is due to arms and not to the leg. Swapping the particle upside down, this is equivalent to a particle with a large number M of legs binding to a uniformly sticky surface, but where on average only 0 or 1 leg is bound to the surface at a time. Therefore, this limit is equivalent to the pre-averaged result, as it should be: each time a new arm is bound it is sampled from its equilibrium distribution – as so many arms are within reach.

Simulations with M arms are presented in Fig. 8-C with analytic solutions Eq. (27) (green colors). They indeed converge to the pre-averaging result (pink). For consistency, we also record the result of Ref. [50] (Eq. (2.48)) that corresponds to pre-averaging *and* assuming $\epsilon = \gamma/\Gamma$. It is plotted in Fig. 8-C (red) and agrees with our result only over a limited range of parameters, corresponding to the validity range of Ref. [50].

4. Numerous legs facing numerous arms

N legs binding to M arms induce a long time effective friction that encapsulates the previous result for M arms and that for N legs in Sec. ID (Supplementary 4.3.4). Eq. (17) still holds with adapted bond probabilities p_n , and γ_{eff} in Eq. (18) is the harmonic average between arm and leg contributions, $(\gamma_{\text{eff},n}(M, N))^{-1} = \gamma_{\text{eff},M,n}^{-1} + \gamma_{\text{eff},N,n}^{-1}$.

Overall, spanning different limits shows that our methodology to investigate long time dynamics is robust, as it accounts for a broad range of physical parameters. It also justifies the use of “pre-averaging” approximations (sampling leg lengths from equilibrium distributions upon binding) to accelerate simulations in specific situations, though it also highlights that taking limits of various parameters is subtle, and care must be taken when doing so as the limits do not commute in general.

CONCLUSION

Nanocaterpillar diffusion is dictated by multiple stochastic events, including binding, unbinding, and leg relaxation, all of which contribute to its macroscale dynamics. We constructed a model for nanocaterpillar motion in one dimension, and showed how to coarse-grain the fast stochastic leg dynamics to obtain an analytic expression for the nanocaterpillar’s long-term effective diffusion coefficient. Our simulations showed this expression is valid over a broad range of parameters, and our experiments using DNA-coated colloids showed this expression is accurate even in a physical system with more

complexity than our model.

We compared our approach to a range of other modeling approaches and assumptions found in the literature, and found our model is the most general, encapsulating other approaches as special limits. In particular, our method justifies approximations used to accelerate simulations in certain situations, such as that upon binding, leg lengths are sampled from their equilibrium distributions [22, 33, 50]. We showed this simulation approach is valid for fast leg dynamics $\gamma/k \ll q_{\text{on}}, q_{\text{off}}$ in 1D, or when binding to a great number of binding partners, such as many arms, $M \gg 1$, yet its validity should be reassessed in more complex geometries.

Our model, though one-dimensional, allows us to distinguish between two modes of motion, sliding and hopping, and to identify parameters that dictate which mode of motion is preferred. Typically, systems with a large number of legs will slide preferentially, since the mean-squared displacement due to hopping decreases exponentially with the number of bound legs. Hopping is favored for systems with short, stiff legs, and/or strong bonds. Regardless of the mode of motion, the fast binding and relaxation dynamics at the microscale result in an overall slow diffusion of the nanocaterpillar.

There are other ways that nanocaterpillars may move macroscopically, beyond hopping and sliding. An important type of motion that our model cannot yet describe is rolling. Rolling has been predicted to lead to a low effective friction, at least in systems with stiff legs, because it doesn’t require stretching legs at the point on a particle which is closest to a sticky surface [33, 53]. While rolling has been modelled in special situations, none of these account for the full stochastic nature of the motion, nor do they systematically derive a coarse-grained equation involving rolling, from microscopic binding and unbinding dynamics [41]. Such a systematic derivation would involve mathematical subtleties beyond those that occur in our work; for example, one would have to consider how rotational and translational degrees of freedom are coupled, and additionally include binding rates with spatial dependencies, to account for the separation between surfaces that is short at the contact point but large further away [75, 76]. Nevertheless, we may expect similar parameters (such as spring relaxation times and unbinding rates) to discriminate between rolling and other modes of motion.

There are numerous additional complexities that could be addressed within our coarse-graining framework. First, details of binding kinetics – that would account *e.g.* for non-exponential kinetics in specific experimental systems [77–79] – could also impact the long time response [42]. Second, mobility of the leg roots – corresponding to fluidity of the bilayer – can be introduced, and may help understand enhanced cohesive motion [10, 80]. Finally, our framework could be extended to account for out-of-equilibrium effects, such as white blood cells streaming in blood flow, or the influenza A virus which has proteins that actively cleave bonds. Ac-

counting for such effects would require adapting bond dynamics to include increased bond rigidity or lifetime in flow [3, 81–85] or memory effects associated with dead zones created by cleaved bonds [26, 36, 51]. Importantly, such improvements require carefully adapting binding rates and bound dynamics to preserve detailed balance when required and other physical constraints [32, 75].

Another important feature that our model does not include in detail is hydrodynamics. Bare friction coefficients (Γ, γ) account for a coarse-grained description of the fluid surrounding the caterpillar and its individual legs. Yet the legs, particle, and wall all interact hydrodynamically in a complex manner. A more detailed model should incorporate how fluid flows within and around the polymer leg mesh. Indeed, elasticity of the polymer mesh could lead to a modification of the particle’s mobility near the interface, as was predicted for particles near elastic membranes [86, 87]. Furthermore, hydrodynamic friction between a particle and a surface depends strongly on the distance between them, an effect known as lubrication or hydrodynamic hindrance, and that is well established for flat rigid walls [88]. The vertical diffusion coefficient of a nanocaterpillar, describing its motion toward and away from a surface, should therefore also include hydrodynamic corrections, taking into account the polymer mesh. Furthermore, stochastic binding and unbinding of the legs also modifies vertical displacements [89] and it is not even clear that a diffusion coefficient would be sufficient to capture the particle’s vertical motion. These questions related to hydrodynamics could lead to important modifications to the theory, and could help shed light on other systems where mobility through fluid is mediated by slender legs, such as for the Vampire amoeba [90].

Beyond its biophysical details, nanocaterpillar motion resonates with other fields where mobility is determined through adhesive contacts. For example, solid state sliding friction is created by bonds breaking between atoms. Close neighbor interactions between bonds, originating from mechanical interactions, can result in dramatic avalanches of bond breaking that change the sliding motion [91, 92]. Similar correlations between nearby bonds could be at play in some nanocaterpillars. For example, in white blood cells, membrane tension mediates bond-bond interactions [47, 48]. It is therefore interesting to speculate whether avalanches of bond unbinding could also occur for nanocaterpillar systems. Overall, the mathematical framework of coarse-graining is well suited to explore how microscopic features determine macroscopic modes of motion for nanocaterpillars and could facilitate predictive capacity for materials design and biophysical systems.

ACKNOWLEDGMENTS

The authors are grateful for fruitful discussions with Fan Cui, Aleksandar Donev, Christopher E. Miles, and David J. Pine. S.M. acknowledges funding from the

MolecularControl project, Horizon 2020 MCSA-IF award number 839225. All authors were supported in part by the MRSEC Program of the National Science Foundation under Award Number DMR-1420073. M.H.-C. was partially supported by the US Department of Energy under Award No. DE-SC0012296, and acknowledges support from the Alfred P. Sloan Foundation.

Appendix A: Projection of the dynamics in the bound state

To project the stochastic dynamics Eqs. (1) and (2) in the bound case we use a formalism (and notation) similar to Ref. [32]; see also [59, 93]. This projection consists in using stiff springs to impose each constraint, and considering the limit where the spring constants go to infinity. The resulting projected equations can be obtained by directly pursuing the steps below (without redoing the reasoning with stiff springs).

We start from stochastic equations in the (x, l) space and seek to project them on the constraint manifold, defined by the constraint $q(x, l) = x + l + x_r = 0$. The constraint matrix is therefore

$$C = (\nabla q)^T = (1 \ 1). \quad (\text{A1})$$

We obtain the projector

$$P = I - C^T(CC^T)^{-1}C = \frac{1}{2} \begin{pmatrix} 1 & -1 \\ -1 & 1 \end{pmatrix}. \quad (\text{A2})$$

Initially the dynamics of $X = (x, l)$ may be written as

$$\frac{dX}{dt} = -\tilde{\Gamma}^{-1}\nabla\mathcal{U}(X) + \sqrt{2k_B T \tilde{\Gamma}^{-1}}\eta_{xl}(t) \quad (\text{A3})$$

where the potential $\mathcal{U}(X) = kl^2/2$, the noise $\eta_{xl} = (\eta_x, \eta_l)$ and the friction matrix is

$$\tilde{\Gamma} = \begin{pmatrix} \Gamma & 0 \\ 0 & \gamma \end{pmatrix}. \quad (\text{A4})$$

The projected friction and its Moore-Penrose pseudo-inverse are

$$\Gamma_P = P\tilde{\Gamma}P = \frac{\Gamma+\gamma}{4} \begin{pmatrix} 1 & -1 \\ -1 & 1 \end{pmatrix}, \quad (\text{A5})$$

$$\Gamma_P^\dagger = \frac{1}{\Gamma+\gamma} \begin{pmatrix} 1 & -1 \\ -1 & 1 \end{pmatrix} \quad (\text{A6})$$

with a square root

$$\sigma_P = \sqrt{\Gamma_P^\dagger} = \frac{1}{\sqrt{\Gamma+\gamma}} \begin{pmatrix} 1 & 0 \\ -1 & 0 \end{pmatrix}. \quad (\text{A7})$$

We obtain the projected dynamics

$$\frac{dX}{dt} = -\Gamma_P^\dagger\nabla\mathcal{U}(X) + \sqrt{2k_B T \Gamma_P^\dagger}\eta_{xl}(t) \quad (\text{A8})$$

where additional terms are needed if C is not constant over the constraint manifold [59, 93]. One can check that this exactly yields the bound dynamics Eq. (3), with $\eta = \eta_x$ (this decomposition of the noise is not unique but this does not impact the dynamics in a weak sense).

Appendix B: Numerical simulations

Stochastic simulations of particle and leg dynamics are conducted using a custom made Fortran 90 routine. Fast random number generation is performed according to a Mersenne twister algorithm. Normally distributed random numbers are used for particle displacement while uniformly distributed random numbers are used to determine binding events. Equations are simulated in their non dimensional form. The step dt was chosen to be much smaller than all other time scales of the system. Typically $dt = \frac{1}{100} \min\left(\frac{q_{\text{on}}\Gamma}{k}, \frac{q_{\text{off}}\Gamma}{k}, \frac{\gamma}{\Gamma}\right)$. The system is simulated for $N_T = 10^8$ time steps, and the simulation is repeated over $N_{\text{runs}} = 100$ independent runs (with renewed random number seed).

To simulate binding and unbinding events, for each leg, at each time step, we choose a random number R uniformly distributed between 0 and 1 and then:

- if the leg is bound, and if $R > q_{\text{off}}dt$ then the leg is unbound. Otherwise it remains bound.
- if the leg is unbound, and if $R > q_{\text{on}}dt$ the leg is bound. Otherwise it remains unbound.

This simulation routine approximates well the exponential binding dynamics expected from the continuous equations since $dt \ll q_{\text{off}}^{-1}, q_{\text{on}}^{-1}$.

To simulate all other stochastic equations we use a standard Euler-Maruyama discretization.

The particle position x is saved every 10^4 time steps, and the mean squared displacement (averaged over initial times $t_0 < (x(t+t_0) - x(t_0))^2 >_{t_0}$) is computed up to $N_T/100 = 10^6$ time steps. The effective diffusion coefficient for each run $D_{\text{eff},i}$ is obtained from the analytic least square regression of $\langle (x(t+t_0) - x(t_0))^2 \rangle_{t_0}$ with time. The average value over the runs $D_{\text{eff}} = \frac{1}{N_{\text{runs}}} \sum_i D_{\text{eff},i}$ is retained as the effective long time diffusion coefficient. The standard deviation of $D_{\text{eff},i}$ allows to draw error bars in all simulation plots.

Appendix C: Diffusion coefficient of DNA-coated colloids

1. Preparation of material

a. DNA coated polystyrene colloids We synthesize DNA-coated polystyrene (PS) spheres using the swelling/deswelling method reported in Ref. [62]. Polystyrene-*b*-poly(ethylene oxide) copolymer PS(3800 g/mol)-*b*-PEO(6500 g/mol) is purchased from Polymer Source Inc, and is first functionalized with azide at the end of the PEO chain [95]. PS-*b*-PEO-N3 are then attached to the PS particles using the swelling/deswelling method. In the synthesis, 15 μL of 1 μm particles (10 w/v, purchased from Thermo Scientific), 125 μL Deionized (DI) water, 160 μL tetrahydrofuran (THF) and

100 μL of PS-*b*-PEO-N3 are mixed at room temperature. The mixture is placed on a horizontal shaker (1000 rpm) for 1.5 hours to fully swell the PS particles and absorb the PS-*b*-PEO-N3 molecules. Then THF is slowly removed from the solution via evaporation by adding DI water, leaving the hydrophobic PS blocks physically inserted into the particles and the hydrophilic PEO chains extending out into the solution. The particles are washed with DI water three times to remove excess polymers.

Single stranded DNA (ssDNA, 20 bases, purchased from Integrated DNA Technogeis) with 5' dibenzocyclooctyne (DBCO) end modification, is clicked to the N3 (at the end of PS-*b*-PEO-N3) through strain promoted alkyne-azide cycloaddition [62]. PS particles previously coated with the PS-*b*-PEO-N3 polymer brush are dispersed in 200 μL of 500 mM PBS buffer, at pH 7.4. Then 10 μL of DBCO-DNA (0.1 mM) are added to the suspension. The mixture is left to react for 48 hours on a horizontal shaker (1000 rpm). The final product is washed in DI water three times and stored in 140 mM PBS buffer. The DNA coverage density is measured using flow cytometry and we obtain $\sigma = 1/(3.27 \text{ nm}^2)$. The DNA sequence used on the colloids is 5'-/DBCO/-T₁₄-ACCGCA-3'.

b. DNA coated glass substrate DNA coated substrates are prepared using the same swelling/deswelling method. First, an ultra thin PS layer is spin-coated to a cleaned 22 mm x 22 mm glass coverslip (purchased from Bioscience Tools). The substrate is then swelled in the same PS-*b*-PEO-N3 solution in THF for 4 hours. Then THF is slowly removed from the solution via evaporation. DNA clicking is performed in a home made PDMS reaction chamber for 48 hours on a shaking stage, then washed 10 times in DI water to remove extra DNA. The entire sample is sealed in the 140 mM PBS buffer (pH 7.4) with 0.3% w/v pluronic F127 surfactants, using UV glue to avoid any external flow or evaporation of the buffer. The DNA sequence used on the glass substrate is complementary to that on the particles, 5'-/DBCO/-T₁₄-TGCGGT-3'.

2. Tracking DNA coated colloids

a. Particle positions measurements To study the diffusion of DNA coated colloids, we track the motion of about 500 particles as they bind and diffuse on the DNA coated substrate – see Fig. 9-A. The sample is mounted on a homemade lab microscope (Nikon Eclipse Ti 60X, 72nm pixel size, depth of focus 560 nm) thermal stage with a temperature controller. Tracer particles fixed on the substrate are used to subtract camera drift during the tracking. Displacement measurements are performed by tracking particles over the temperature range 28-62 °C – see Fig. 9-B. At each temperature, particles are tracked over a time range of 20 min at a frame rate of 5 images per second. For the highest temperature reported here, $T = 59.1$ °C, particles diffuse faster and we only track

Parameter	Value at T_m	Method and References
Γ	1.6×10^{-8} N.s/m	hydrodynamic friction near a surface $\Gamma = 2 \times 6\pi\eta R$; colloid radius $R = 500$ nm [31]; $\eta(T)$ water viscosity with temperature.
γ	1.8×10^{-10} N.s/m	$\gamma = 6\pi\eta(T)h$; brush height $h \simeq 22$ nm, calculated with Milner-Witten-Cates theory [64], and accounting for increased brush density due to Pluronic F127 (see Ref. [38]); slightly dependent on T
k	0.16 mN/m	$k = 3k_B T / 2L\ell$, spring constant for polymers [55]; extended brush length $L \simeq 84$ nm (6500 g/mol PEO + 20 single stranded DNA (ssDNA) bases); persistence length $\ell = 0.5$ nm (average of PEO + ssDNA at 140 mM salt concentration [94])
q_{on}	4 kHz	$q_{\text{on}} = k_{\text{on}}\bar{\sigma}/h\mathcal{N}_A$; $k_{\text{on}} = 1.6 \times 10^6$ M $^{-1}$.s $^{-1}$ from Ref. [63], using the exact sequence as in our experiments; $\bar{\sigma} = \sqrt{\sigma\sigma_g}$ where $\sigma = 1/(3.27 \text{ nm})^2$ is the particle coating density and $\sigma_g = 1/(10.8 \text{ nm})^2$ is the glass substrate coating density; Avogadro's number \mathcal{N}_A ; Independent of T .
q_{off}	18 kHz	$q_{\text{off}} = q_{\text{on}} \frac{N(T) - N_b(T)}{N_b(T)}$; N_b average bound fraction, N number of legs available for binding in the interaction region

TABLE II. Method used to calculate model parameters for the DNA coated colloids studied experimentally in this work. Parameter values are reported only at the melting temperature T_m . Their dependence on temperature is highlighted in the method column.

them over 5 min, with 10 images per second. Images are then analyzed using the TrackPy software to obtain individual particle positions with time. Particles that do not move at all even at high temperatures are removed from the analysis. These particles are likely in a low density area where steric repulsion is not sufficient to screen van der Waals attraction, and therefore are “crashed” on the surface.

b. Melting curve To obtain the fraction of bound and unbound particles we use a similar thermodynamic approach as in Ref. [38]. At the lowest recorded temperature we count the average total number of particles in focus per frame say N_{tot} . For each higher temperature we count the average number of particles in focus per frame say N_T . We then obtain the percentage of bound particles as N_T/N_{tot} and of unbound particles as $1 - N_T/N_{\text{tot}}$. This approach effectively counts the number of particles within typically 280 nm (half the depth of focus) from the surface. At high temperatures some particles remain close to the surface due to gravity.

c. Mean square displacement analysis We fit the ensemble mean-squared displacement to a power law as $\langle x^2(t) \rangle = 4Dt^\alpha$ using a linear regression in log space to get the diffusion coefficient D and the power on time α . For temperatures above 54.8 °C we obtained $1.02 > \alpha > 0.96$. We then fix $\alpha = 1$ for these high temperatures to obtain the D data as reported in Fig. 7-C.

3. Modeling tools for DNA-coated colloids

In general the particle can explore positions far from the surface, where binding is not possible. To account for this 2D geometry, that is especially important for our DNA-coated colloids that can venture far from the surface when they are unbind due to buoyancy, we use an extension of our main model.

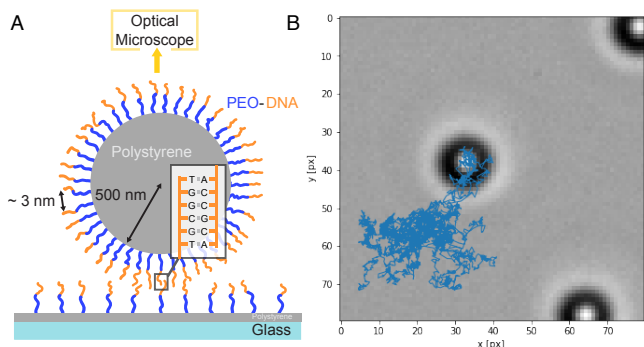


FIG. 9. **Experimental setup to measure diffusion of DNA-coated colloids on DNA-coated surfaces.** (A) Schematic of a DNA-coated colloid attaching to a DNA-coated substrate, with the specific DNA sequence used in this study. Diffusion of the colloids is tracked from on-top. (B) Example of a colloid trajectory over a 18 min time frame (in blue) overlaid on the bright-field microscope image corresponding to the colloid’s initial position. Here 1 px corresponds to 0.108 μm .

One option to account for such a 2D dependence is to add a vertical degree of freedom say y for the particle, together with spatially dependent rates $q_{\text{on}}(y), q_{\text{off}}(y)$. This is not a trivial modification, especially as there are different ways to set the spatial dependence y of $q_{\text{on}}(y), q_{\text{off}}(y)$ (see for example the variability between Refs. [49, 50, 72]).

Instead we rely on a simplified approach, that has been shown to accurately account for 2D geometry in another context [96], where we describe the system with $2 \times 1\text{D}$ lines. For a 1-legged particle, we consider that the particle can switch between two regions where its dynamics are constrained to 1D: surface and bulk regions. The particle enters the surface region with rate Q_{on} , and then can bind to the surface with rate q_{on} . If the particle is

unbound in the surface region, it may lift off from the surface region to the bulk region with rate Q_{off} . $\frac{Q_{\text{on}}}{Q_{\text{off}}}$ corresponds to the ratio of positions where the receptors are within and beyond reach. In DNA-coated colloid explorations, where particles are considered on top of a sticky surface, the ratio can be small or large depending on the density mismatch between the particle material and the surrounding fluid, and hence the particle's gravitational height [39]. For other systems, such as white blood cells that are confined within blood vessels, particles are always close to the wall [97] and hence the ratio is quite large. Approach and lift-off from the surface are slow processes that scale like the diffusive dynamics of the particle and thus we may assume $Q_i\tau \sim O_\epsilon(1)$.

Performing similar coarse-graining steps (Supplementary 2), we obtain an effective friction

$$\frac{1}{\Gamma_{\text{eff}}^{2 \times 1D}} = \frac{p_0^{2 \times 1D}}{\Gamma_0} + \frac{p_1^{2 \times 1D}}{\Gamma_1} \quad (\text{C1})$$

where the probability to be in either states takes into account the added degree of freedom, $p_1^{2 \times 1D} = Q_{\text{on}}q_{\text{on}}/Z$ and $p_0^{2 \times 1D} = q_{\text{off}}(Q_{\text{on}} + Q_{\text{off}})/Z$ with Z a normalization

constant such that $p_0^{2 \times 1D} + p_1^{2 \times 1D} = 1$. The added degree of freedom does not change the result of Eq. (14), simply the mathematical interpretation of the probability factors. Note that this framework has been verified against numerical simulations.

The values of Q_{on} and Q_{off} can be evaluated from the detailed interaction potential $\phi(h)$ of a DNA-coated colloid and the surface (see Sec. II). In fact, the probability to be near the surface, in the absence of binding, is measured by

$$\frac{Q_{\text{on}}}{Q_{\text{on}} + Q_{\text{off}}} = \int_0^{h_p} e^{-\beta(\phi(h) - \phi_{\text{bind}}(h))} dh / Z \quad (\text{C2})$$

where $\phi_{\text{bind}}(h)$ measures the contributions to the interaction potential due to binding, $h_p \simeq 20$ nm measures the typical width of attractive interactions (region of space where binding could happen) and Z is a normalizing factor. $\frac{Q_{\text{on}}}{Q_{\text{on}} + Q_{\text{off}}} \simeq 0.0015$ and does not depend much on temperature. It also does not depend significantly on the exact value of h_p for $h_p = 2 - 40$ nm. Other parameters entering the calculation of D_{eff} are detailed in Table. II.

-
- [1] M. Mammen, S.-K. Choi, and G. M. Whitesides, Multivalent interactions in biological systems: implications for design and use of multivalent ligands and inhibitors, *Angewandte Chemie International Edition* **37**, 2754 (1998).
- [2] P. C. Bressloff and J. M. Newby, Stochastic models of intracellular transport, *Reviews of Modern Physics* **85**, 135 (2013).
- [3] D. A. Hammer, Adhesive dynamics, *Journal of biomechanical engineering* **136**, 021006 (2014).
- [4] W. B. Rogers, W. M. Shih, and V. N. Manoharan, Using dna to program the self-assembly of colloidal nanoparticles and microparticles, *Nature Reviews Materials* **1**, 1 (2016).
- [5] R. Alon and S. Feigelson, From rolling to arrest on blood vessels: leukocyte tap dancing on endothelial integrin ligands and chemokines at sub-second contacts, in *Seminars in immunology*, Vol. 14 (Elsevier, 2002) pp. 93–104.
- [6] K. Ley, C. Laudanna, M. I. Cybulsky, and S. Nourshargh, Getting to the site of inflammation: the leukocyte adhesion cascade updated, *Nature Reviews Immunology* **7**, 678 (2007).
- [7] C. Korn and U. Schwarz, Dynamic states of cells adhering in shear flow: from slipping to rolling, *Physical review E* **77**, 041904 (2008).
- [8] Y. Zhang, A. McMullen, L.-L. Pontani, X. He, R. Sha, N. C. Seeman, J. Brujic, and P. M. Chaikin, Sequential self-assembly of dna functionalized droplets, *Nature communications* **8**, 1 (2017).
- [9] L.-L. Pontani, I. Jorjadze, and J. Brujic, Cis and trans cooperativity of e-cadherin mediates adhesion in biomimetic lipid droplets, *Biophysical journal* **110**, 391 (2016).
- [10] S. Merminod, J. R. Edison, H. Fang, M. F. Hagan, and W. B. Rogers, Avidity and surface mobility in multivalent ligand-receptor binding, *Nanoscale* (2021).
- [11] R. J. Macfarlane, B. Lee, M. R. Jones, N. Harris, G. C. Schatz, and C. A. Mirkin, Nanoparticle superlattice engineering with dna, *science* **334**, 204 (2011).
- [12] D. J. Lewis, L. Z. Zornberg, D. J. Carter, and R. J. Macfarlane, Single-crystal winterbottom constructions of nanoparticle superlattices, *Nature materials* **19**, 719 (2020).
- [13] J.-G. Park, S.-H. Kim, S. Magkiriadou, T. M. Choi, Y.-S. Kim, and V. N. Manoharan, Full-spectrum photonic pigments with non-iridescent structural colors through colloidal assembly, *Angewandte Chemie International Edition* **53**, 2899 (2014).
- [14] M. He, J. P. Gales, É. Ducrot, Z. Gong, G.-R. Yi, S. Sacanna, and D. J. Pine, Colloidal diamond, *Nature* **585**, 524 (2020).
- [15] R. Merindol, N. Martin, T. Beneyton, J.-C. Baret, and S. Ravaine, Fast and ample light controlled actuation of monodisperse all-dna microgels, *Advanced Functional Materials* **31**, 2010396 (2021).
- [16] C. R. Bilchak, M. Jhalaria, Y. Huang, Z. Abbas, J. Midya, F. M. Benedetti, D. Parisi, W. Egger, M. Dickmann, M. Minelli, *et al.*, Tuning selectivities in gas separation membranes based on polymer-grafted nanoparticles, *ACS nano* **14**, 17174 (2020).
- [17] T. Sakai, S. I. Nishimura, T. Naito, and M. Saito, Influenza a virus hemagglutinin and neuraminidase act as novel motile machinery, *Scientific reports* **7**, 1 (2017).
- [18] T. Sakai, H. Takagi, Y. Muraki, and M. Saito, Unique directional motility of influenza c virus controlled by its filamentous morphology and short-range motions, *Journal of virology* **92**, e01522 (2018).
- [19] M. Müller, D. Lauster, H. H. Wildenauer, A. Herrmann,

- and S. Block, Mobility-based quantification of multivalent virus-receptor interactions: New insights into influenza a virus binding mode, *Nano letters* **19**, 1875 (2019).
- [20] T. D. Allen, J. Cronshaw, S. Bagley, E. Kiseleva, and M. W. Goldberg, The nuclear pore complex: mediator of translocation between nucleus and cytoplasm, *Journal of cell science* **113**, 1651 (2000).
- [21] I. V. Aramburu and E. A. Lemke, Floppy but not sloppy: Interaction mechanism of fg-nucleoporins and nuclear transport receptors, in *Seminars in cell & developmental biology*, Vol. 68 (Elsevier, 2017) pp. 34–41.
- [22] B. Fogelson and J. P. Keener, Enhanced nucleocytoplasmic transport due to competition for elastic binding sites, *Biophysical journal* **115**, 108 (2018).
- [23] R. Alon, S. Chen, K. D. Puri, E. B. Finger, and T. A. Springer, The kinetics of l-selectin tethers and the mechanics of selectin-mediated rolling, *The Journal of cell biology* **138**, 1169 (1997).
- [24] R. Shrivastava, A. Rai, M. Salapaka, and S. Sivaramakrishnan, Stiffness of cargo–motor linkage tunes myosin vi motility and response to load, *Biochemistry* **58**, 4721 (2019).
- [25] A. K. Dasanna and U. S. Schwarz, Adhesion-based sorting of blood cells: an adhesive dynamics simulation study, *Soft matter* **14**, 9061 (2018).
- [26] K. Yehl, A. Mugler, S. Vivek, Y. Liu, Y. Zhang, M. Fan, E. R. Weeks, and K. Salaita, High-speed dna-based rolling motors powered by rnase h, *Nature nanotechnology* **11**, 184 (2016).
- [27] R. Karnik, S. Hong, H. Zhang, Y. Mei, D. G. Anderson, J. M. Karp, and R. Langer, Nanomechanical control of cell rolling in two dimensions through surface patterning of receptors, *Nano letters* **8**, 1153 (2008).
- [28] Y.-Y. Wang, A. Kannan, K. L. Nunn, M. A. Murphy, D. B. Subramani, T. Moench, R. Cone, and S. K. Lai, Igg in cervicovaginal mucus traps hsv and prevents vaginal herpes infections, *Mucosal immunology* **7**, 1036 (2014).
- [29] A. Hensley, W. M. Jacobs, and W. B. Rogers, Classical nucleation and growth of dna-programmed colloidal crystallization, arXiv preprint arXiv:2105.14631 (2021).
- [30] D. J. Lewis, P. A. Gabrys, and R. J. Macfarlane, Dna-directed non-langmuir deposition of programmable atom equivalents, *Langmuir* **34**, 14842 (2018).
- [31] Y. Wang, Y. Wang, X. Zheng, É. Ducrot, J. S. Yodh, M. Weck, and D. J. Pine, Crystallization of dna-coated colloids, *Nature communications* **6**, 1 (2015).
- [32] M. Holmes-Cerfon, Stochastic disks that roll, *Physical Review E* **94**, 052112 (2016).
- [33] P. K. Jana and B. M. Mognetti, Translational and rotational dynamics of colloidal particles interacting through reacting linkers, *Physical Review E* **100**, 060601 (2019).
- [34] C. Loverdo, O. Benichou, R. Voituriez, A. Biebricher, I. Bonnet, and P. Desbailles, Quantifying hopping and jumping in facilitated diffusion of dna-binding proteins, *Physical review letters* **102**, 188101 (2009).
- [35] P. E. Hamming, N. J. Overeem, and J. Huskens, Influenza as a molecular walker, *Chemical science* **11**, 27 (2019).
- [36] M. D. Vahey and D. A. Fletcher, Influenza a virus surface proteins are organized to help penetrate host mucus, *Elife* **8**, e43764 (2019).
- [37] K. Ramesh, R. Thaokar, J. R. Prakash, and R. Prabhakar, Significance of thermal fluctuations and hydrodynamic interactions in receptor-ligand-mediated adhesive dynamics of a spherical particle in wall-bound shear flow, *Physical Review E* **91**, 022302 (2015).
- [38] F. Cui, S. Marbach, J. Zheng, M. Holmes-Cerfon, and D. S. Pine, Comprehensive microscopic view of binding between dna-coated colloids, to appear (2021).
- [39] Q. Xu, L. Feng, R. Sha, N. Seeman, and P. Chaikin, Subdiffusion of a sticky particle on a surface, *Physical review letters* **106**, 228102 (2011).
- [40] C. Etchegaray and N. Meunier, A stochastic model for cell adhesion to the vascular wall, *Journal of mathematical biology* **79**, 1665 (2019).
- [41] F. Ziebert and I. M. Kulić, How influenza’s spike motor works, *Physical Review Letters* **126**, 218101 (2021).
- [42] N. A. Licata and A. V. Tkachenko, Colloids with key-lock interactions: Nonexponential relaxation, aging, and anomalous diffusion, *Physical Review E* **76**, 041405 (2007).
- [43] S. Bose, S. K. Das, J. M. Karp, and R. Karnik, A semi-analytical model to study the effect of cortical tension on cell rolling, *Biophysical journal* **99**, 3870 (2010).
- [44] A. Kowalewski, N. R. Forde, and C. S. Korosec, Multivalent diffusive transport, *The Journal of Physical Chemistry B* (2021).
- [45] K. E. Caputo and D. A. Hammer, Effect of microvillus deformability on leukocyte adhesion explored using adhesive dynamics simulations, *Biophysical journal* **89**, 187 (2005).
- [46] B. Grec, B. Maury, N. Meunier, and L. Navoret, A 1d model of leukocyte adhesion coupling bond dynamics with blood velocity, *Journal of theoretical biology* **452**, 35 (2018).
- [47] S. Klumpp and R. Lipowsky, Cooperative cargo transport by several molecular motors, *Proceedings of the National Academy of Sciences* **102**, 17284 (2005).
- [48] S. F. Fenz, T. Bihl, D. Schmidt, R. Merkel, U. Seifert, K. Sengupta, and A.-S. Smith, Membrane fluctuations mediate lateral interaction between cadherin bonds, *Nature physics* **13**, 906 (2017).
- [49] C. P. Goodrich, M. P. Brenner, and K. Ribbeck, Enhanced diffusion by binding to the crosslinks of a polymer gel, *Nature communications* **9**, 1 (2018).
- [50] B. Fogelson and J. P. Keener, Transport facilitated by rapid binding to elastic tethers, *SIAM Journal on Applied Mathematics* **79**, 1405 (2019).
- [51] C. S. Korosec, L. Jindal, M. Schneider, I. C. de la Barca, M. J. Zuckermann, N. R. Forde, and E. Emberly, Substrate stiffness tunes the dynamics of polyvalent rolling motors, *Soft Matter* **17**, 1468 (2021).
- [52] G. Pavliotis and A. Stuart, *Multiscale methods: averaging and homogenization* (Springer Science & Business Media, 2008).
- [53] J. P. Lee-Thorp and M. Holmes-Cerfon, Modeling the relative dynamics of dna-coated colloids, *Soft matter* **14**, 8147 (2018).
- [54] X. Bian, C. Kim, and G. E. Karniadakis, 111 years of brownian motion, *Soft Matter* **12**, 6331 (2016).
- [55] M. Rubinstein, R. H. Colby, *et al.*, *Polymer physics*, Vol. 23 (Oxford university press New York, 2003).
- [56] E. Miller, T. Garcia, S. Hultgren, and A. F. Oberhauser, The mechanical properties of e. coli type 1 pili measured by atomic force microscopy techniques, *Biophysical journal* **91**, 3848 (2006).
- [57] R. Y. Lim, N.-P. Huang, J. Köser, J. Deng, K. A. Lau,

- K. Schwarz-Herion, B. Fahrenkrog, and U. Aebi, Flexible phenylalanine-glycine nucleoporins as entropic barriers to nucleocytoplasmic transport, *Proceedings of the National Academy of Sciences* **103**, 9512 (2006).
- [58] P. Varilly, S. Angioletti-Uberti, B. M. Mognetti, and D. Frenkel, A general theory of dna-mediated and other valence-limited colloidal interactions, *The Journal of chemical physics* **137**, 094108 (2012).
- [59] G. Ciccotti, T. Lelievre, and E. Vanden-Eijnden, Projection of diffusions on submanifolds: Application to mean force computation, *Communications on Pure and Applied Mathematics: A Journal Issued by the Courant Institute of Mathematical Sciences* **61**, 371 (2008).
- [60] C. W. Gardiner *et al.*, *Handbook of stochastic methods*, Vol. 3 (Springer Berlin, 1985).
- [61] L. Leibler, M. Rubinstein, and R. H. Colby, Dynamics of reversible networks, *Macromolecules* **24**, 4701 (1991).
- [62] J. S. Oh, Y. Wang, D. J. Pine, and G.-R. Yi, High-density pco-b-dna brushes on polymer particles for colloidal superstructures, *Chemistry of Materials* **27**, 8337 (2015).
- [63] J. X. Zhang, J. Z. Fang, W. Duan, L. R. Wu, A. W. Zhang, N. Dalchau, B. Yordanov, R. Petersen, A. Phillips, and D. Y. Zhang, Predicting dna hybridization kinetics from sequence, *Nature chemistry* **10**, 91 (2018).
- [64] S. T. Milner, T. A. Witten, and M. E. Cates, Theory of the grafted polymer brush, *Macromolecules* **21**, 2610 (1988).
- [65] The binding range is about 20 nm, but this is not optically removable as the vertical resolution is about 200 nm.
- [66] W. Cao, C. Dong, S. Kim, D. Hou, W. Tai, L. Du, W. Im, and X. F. Zhang, Biomechanical characterization of sars-cov-2 spike rbd and human ace2 protein-protein interaction, *Biophysical journal* **120**, 1011 (2021).
- [67] M. Ponga, Quantifying the adhesive strength between the sars-cov-2 s-proteins and human receptor and its effect in therapeutics, *Scientific reports* **10**, 1 (2020).
- [68] A. Harris, G. Cardone, D. C. Winkler, J. B. Heymann, M. Brecher, J. M. White, and A. C. Steven, Influenza virus pleiomorphy characterized by cryoelectron tomography, *Proceedings of the National Academy of Sciences* **103**, 19123 (2006).
- [69] V. Reiter-Scherer, J. L. Cuellar-Camacho, S. Bhatia, R. Haag, A. Herrmann, D. Lauster, and J. P. Rabe, Force spectroscopy shows dynamic binding of influenza hemagglutinin and neuraminidase to sialic acid, *Biophysical journal* **116**, 1037 (2019).
- [70] Eq. (22) corresponds to the result derived in Ref. [53], with in addition projected dynamics are considered in the bound state, and base friction of the particle ($\Gamma \neq 0$).
- [71] S. Marbach and M. Holmes-Cerfon, Inertial effects for particles with multivalent ligand receptor, submitted to *Phys. Rev. E* (2021).
- [72] C. Fröhner and F. Noé, Reversible interacting-particle reaction dynamics, *The Journal of Physical Chemistry B* **122**, 11240 (2018).
- [73] S. Xu, J. Zhan, B. Man, S. Jiang, W. Yue, S. Gao, C. Guo, H. Liu, Z. Li, J. Wang, *et al.*, Real-time reliable determination of binding kinetics of dna hybridization using a multi-channel graphene biosensor, *Nature communications* **8**, 1 (2017).
- [74] K.-C. Chang, D. F. Tees, and D. A. Hammer, The state diagram for cell adhesion under flow: leukocyte rolling and firm adhesion, *Proceedings of the National Academy of Sciences* **97**, 11262 (2000).
- [75] C. Korn and U. Schwarz, Mean first passage times for bond formation for a brownian particle in linear shear flow above a wall, *The Journal of chemical physics* **126**, 03B605 (2007).
- [76] U. S. Schwarz and R. Alon, L-selectin-mediated leukocyte tethering in shear flow is controlled by multiple contacts and cytoskeletal anchorage facilitating fast rebinding events, *Proceedings of the National Academy of Sciences* **101**, 6940 (2004).
- [77] M. I. Wallace, L. Ying, S. Balasubramanian, and D. Klennerman, Non-arrhenius kinetics for the loop closure of a dna hairpin, *Proceedings of the National Academy of Sciences* **98**, 5584 (2001).
- [78] W. B. Rogers, T. Sinno, and J. C. Crocker, Kinetics and non-exponential binding of dna-coated colloids, *Soft Matter* **9**, 6412 (2013).
- [79] K.-T. Wu, L. Feng, R. Sha, R. Dreyfus, A. Y. Grosberg, N. C. Seeman, and P. M. Chaikin, Kinetics of dna-coated sticky particles, *Physical Review E* **88**, 022304 (2013).
- [80] N. Sarpangala and A. Gopinathan, Cargo surface fluidity reduces inter-motor interference, promotes load-sharing and enhances run-lengths in an atp dependent manner, *bioRxiv* (2021).
- [81] G. I. Bell, Models for the specific adhesion of cells to cells, *Science* **200**, 618 (1978).
- [82] P. S. Doyle, B. Ladoux, and J.-L. Viovy, Dynamics of a tethered polymer in shear flow, *Physical review letters* **84**, 4769 (2000).
- [83] S. Chen and T. A. Springer, Selectin receptor–ligand bonds: Formation limited by shear rate and dissociation governed by the bell model, *Proceedings of the National Academy of Sciences* **98**, 950 (2001).
- [84] D. E. Leckband, Novel functions and binding mechanisms of carbohydrate-binding proteins determined by force measurements, *Current Protein and Peptide Science* **12**, 743 (2011).
- [85] S. Rakshit and S. Sivasankar, Biomechanics of cell adhesion: how force regulates the lifetime of adhesive bonds at the single molecule level, *Physical Chemistry Chemical Physics* **16**, 2211 (2014).
- [86] A. Daddi-Moussa-Ider, A. Guckenberger, and S. Gekle, Long-lived anomalous thermal diffusion induced by elastic cell membranes on nearby particles, *Physical Review E* **93**, 012612 (2016).
- [87] V. Bertin, Y. Amarouchene, E. Raphael, and T. Salez, Soft-lubrication interactions between a rigid sphere and an elastic wall, *arXiv preprint arXiv:2104.00900* (2021).
- [88] H. Brenner, The slow motion of a sphere through a viscous fluid towards a plane surface, *Chemical Engineering Science* **16**, 242 (1961).
- [89] M. Mani, A. Gopinath, and L. Mahadevan, How Things Get Stuck: Kinetics, Elastohydrodynamics, and Soft Adhesion, *Physical Review Letters* **108**, 226104 (2012).
- [90] S. Hess, N. Sausen, and M. Melkonian, Shedding light on vampires: the phylogeny of vampyrellid amoebae revisited, *PLoS One* **7**, e31165 (2012).
- [91] T. W. de Geus, M. Popović, W. Ji, A. Rosso, and M. Wyart, How collective asperity detachments nucleate slip at frictional interfaces, *Proceedings of the National Academy of Sciences* **116**, 23977 (2019).
- [92] W. Ji, T. W. de Geus, E. Agoritsas, and M. Wyart, Geometry of hopping processes and local excitations in glasses, *arXiv preprint arXiv:2106.13153* (2021).

- [93] M. Holmes-Cerfon, S. J. Gortler, and M. P. Brenner, A geometrical approach to computing free-energy landscapes from short-ranged potentials, *Proceedings of the National Academy of Sciences* **110**, E5 (2013).
- [94] H. Chen, S. P. Meisburger, S. A. Pabit, J. L. Sutton, W. W. Webb, and L. Pollack, Ionic strength-dependent persistence lengths of single-stranded RNA and DNA, *Proceedings of the National Academy of Sciences* **109**, 799 (2012).
- [95] S. Hiki and K. Kataoka, A facile synthesis of azido-terminated heterobifunctional poly (ethylene glycol) s for “click” conjugation, *Bioconjugate chemistry* **18**, 2191 (2007).
- [96] S. Marbach, Intrinsic fractional noise in nanopores: The effect of reservoirs, *The Journal of Chemical Physics* **154**, 171101 (2021).
- [97] C. Sun, C. Migliorini, and L. L. Munn, Red blood cells initiate leukocyte rolling in postcapillary expansions: a lattice boltzmann analysis, *Biophysical journal* **85**, 208 (2003).